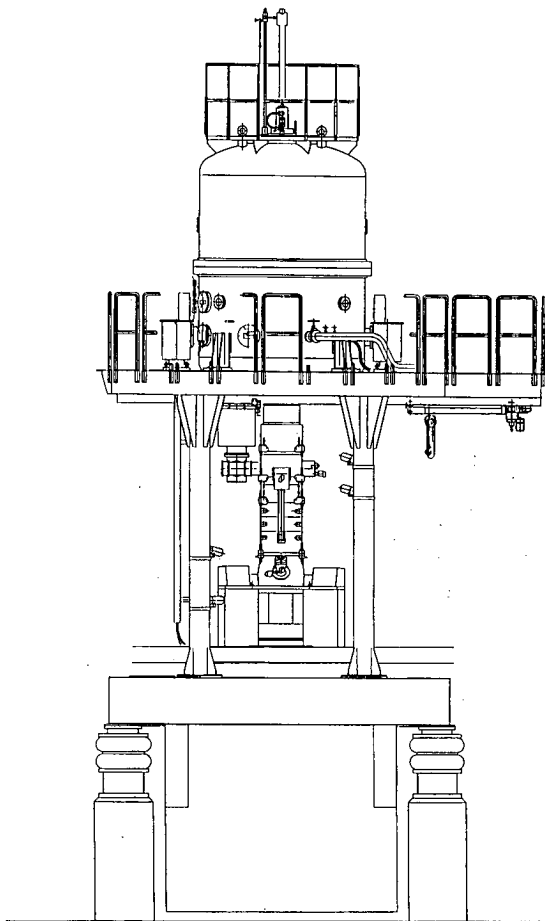


## **DISCLAIMER**

This document was prepared as an account of work sponsored by the United States Government. While this document is believed to contain correct information, neither the United States Government nor any agency thereof, nor the Regents of the University of California, nor any of their employees, makes any warranty, express or implied, or assumes any legal responsibility for the accuracy, completeness, or usefulness of any information, apparatus, product, or process disclosed, or represents that its use would not infringe privately owned rights. Reference herein to any specific commercial product, process, or service by its trade name, trademark, manufacturer, or otherwise, does not necessarily constitute or imply its endorsement, recommendation, or favoring by the United States Government or any agency thereof, or the Regents of the University of California. The views and opinions of authors expressed herein do not necessarily state or reflect those of the United States Government or any agency thereof or the Regents of the University of California.

# *Current Titles*

*National Center for Electron Microscopy*



REFERENCE COPY  
Does Not  
Circulate

Bldg. 50 Library.

Copy 1

PUB-719

---

---

July 1995

---

---

#### DISCLAIMER

This document was prepared as an account of work sponsored by the United States Government. Neither the United States Government nor any agency thereof, nor The Regents of the University of California, nor any of their employees, makes any warranty, express or implied, or assumes any legal liability or responsibility for the accuracy, completeness, or usefulness of any information, apparatus, product, or process disclosed, or represents that its use would not infringe privately owned rights. Reference herein to any specific commercial product, process, or service by its trade name, trademark, manufacturer, or otherwise, does not necessarily constitute or imply its endorsement, recommendation, or favoring by the United States Government or any agency thereof, or The Regents of the University of California. The views and opinions of authors expressed herein do not necessarily state or reflect those of the United States Government or any agency thereof or The Regents of the University of California and shall not be used for advertising or product endorsement purposes.

Lawrence Berkeley Laboratory is an equal opportunity employer.

---

---

---

---

National Center for Electron Microscopy  
U.C. Lawrence Berkeley Laboratory  
1 Cyclotron Rd. Building 72  
Berkeley CA 94720

---

---

---

---

National Center for Electron Microscopy  
U.C. Lawrence Berkeley Laboratory  
1 Cyclotron Rd. Building 72  
Berkeley CA 94720

Please send a reprint of the paper(s):

Number	Author(s)	Title

Name\_\_\_\_\_ Date\_\_\_\_\_

Affiliation\_\_\_\_\_

Address\_\_\_\_\_

\_\_\_\_\_

Please send a reprint of the paper(s);

Number	Author(s)	Title

Name\_\_\_\_\_ Date\_\_\_\_\_

Affiliation\_\_\_\_\_

Address\_\_\_\_\_

\_\_\_\_\_

# *Current Titles*

National Center for Electron Microscopy  
Lawrence Berkeley Laboratory  
University of California  
Berkeley, California 94720

July 1995

PUB-719

For current information about the NCEM  
see our www page at

***<http://ncem.lbl.gov/ncem.html>***

The NCEM is supported by the Director, Office of Energy Research, Office of Basic Energy Sciences, Materials Sciences Division of the U.S. Department of Energy under Contract No. DE-AC03-76SF00098.

This booklet is published for those interested in current research being conducted at the National Center for Electron Microscopy. The NCEM is a DOE-designated national user facility and is available at no charge to qualified researchers. Access is controlled by an external steering committee. Interested researchers may contact Gretchen Hermes at (510) 486-5006 or address below for a User's Guide.

Copies of available papers can be ordered from:

Theda Crawford  
National Center for Electron Microscopy  
Lawrence Berkeley Laboratory  
One Cyclotron Rd., MS72  
Berkeley, California, USA 94720

**Articles are listed alphabetically by journal.**

**Legend:**

Number = publication number

R = Reprints

P = Preprints

No = None available

Pub475Rev.93            M            P

edited by J. Turner

## **NCEM User's Guide**

1993

User's guide to the National Center for Electron Microscopy, Lawrence Berkeley Laboratory, University of California, Berkeley.

---

PUB658                    M            P

M.A. O'Keefe and R. Kilaas

## **NCEMSS Manual**

NCEM Prog. (HRTEM)    1994

Manual for the National Center for Electron Microscopy Simulation System for the simulation of HRTEM images.

### **Quantitative HREM of Interfaces Through Image Processing**

#### **3rd Interamerican Congress on EM**

One of the main efforts in the field of high resolution electron microscopy is to make the technique more quantitative. Of the various approaches, digital image processing and simulation, as well as image matching have assumed a preeminent role. This work describes the application of these techniques to the quantitative analysis of a near- $\Sigma 5$  (210) grain boundary in Rutile. Simulations were carried out using MacTempas (total resolution). Image analysis was done under Digital Micrograph (Gatan, Inc.) for which a set of custom functions was developed to implement pattern recognition, peak finding, and non-periodic lattice averaging. The grain boundary was imaged using the Lawrence Berkeley Lab ARM, at 800 kV.

### **Dynamic Observations of Pore Growth in Silicon**

#### **5th Frontiers**

The recent (1990) discovery that anodically etched silicon can luminesce in the red part of the visible spectrum created an immense amount of interest in this fascinating material. Activity initially centered around the possibility of using porous silicon in electroluminescent devices, thereby finally achieving the aim of optoelectronic integration. However, this unusual material is also of interest as molecular sieves, filters and catalyst supports. These diverse applications depend on the microscopic details of the pores formed during the etching process, which as a function of the doping level and the etching conditions, can range from micron-sized straight channels of arbitrary aspect ratio to sub-nanometer, non-directional branched structures.

## **Extending the Resolution of the HRTEM by Image Processing**

### **5th Frontiers**

The resolution of a high-resolution transmission electron microscope (HRTEM) has traditionally been defined in terms of its Scherzer resolution limit at optimum defocus. However, even beyond Scherzer limit, spatial frequencies can be transferred from the specimen to the image, out to the information limit of the electron microscope, which is determined largely by the amount of energy spread in the electron beam. The best microscope resolutions have been limited to approximately  $1.6\text{\AA}$  (at least until recently). To improve beyond this value requires either an increase in voltage (to reduce the electron wavelength), spherical aberration compensation (to improve the Scherzer resolution), or a method of exploiting the information existing in the spatial frequency band that falls beyond the Scherzer resolution but inside the microscope information limit. Scherzer resolution occurs at the highest spatial frequency that can be transferred into the image with the same phase as all lower frequencies. The information limit is the highest spatial frequency that can be transferred with significant amplitude regardless of any phase differences with respect to lower frequencies. With suitable computer processing of a focal series of images, misphased frequencies can be corrected, and an aggregate image produced that mimics a Scherzer image, but with a resolution that approaches the information limit.

---

## **An HREM Analysis of Unusual Precipitate Morphologies in $\text{MoSi}_2$**

### **5th Frontiers**

Two different morphologies of  $\text{Mo}_5\text{Si}_3$  precipitates have been observed in a  $\text{MoSi}_2$  single crystal matrix. Both types of precipitate are laths elongated along the  $[110]$  direction common to the matrix and the precipitate structure. However, their orientation relationships and shapes in cross section, normal to the lath axis, are characteristically different.

---

35856

A

No

M.A. O'Keefe and V. Radmilovic

### **Specimen Thickness Derived from Matching with Simulated Images is Under Estimated**

5th Frontiers

Simulated high-resolution transmission electron microscope (HRTEM) images can accurately reproduce experimental HRTEM images only when imaging parameters are accurately known. The most difficult parameter to measure, and thus to include accurately in the image simulation is the specimen thickness. In matches of experimental and simulated HRTEM images, specimen thickness is sometimes treated as a disposable parameters, i.e., the experimental specimen thickness is not measured, but assumed to be the thickness at which the simulation program produces a simulated image that best matches the experimental one. Such a procedure can result in seriously underestimated specimen thicknesses. Often the matching thickness at the known defocus is ridiculously small and a greater thickness is chosen by incorrectly estimating the defocus; this mistake is possible because of the natural trade-off between objective lens defocus and specimen thickness, as shown in image maps. Simulated images change more rapidly than experimental ones with increasing crystal thickness because simulated scattering is more dynamical than experimental scattering, i.e., with increasing thickness, simulated images attain a specific image character faster than do experimental ones because simulated specimens are usually positioned exactly on-axis and experimental specimens are not.

---

37086

M

No

F.M. Ross and P.C. Searson

### **Dynamic Observation of Electrochemical Etching in Silicon**

9th Int'l. Mic. Semicon. Mats.

We have designed and constructed a TEM specimen holder in order to observe the process of pore formation in silicon. The holder incorporates electrical feedthroughs and a sealed reservoir for the electrolyte and accepts lithographically patterned silicon specimens. We describe the system and present preliminary, ex situ observations of the etching process.

---

un-numbered

M

No

A. Claverie, H. Fujioka, L. Laanab, Z. Liliental-Weber and E.R. Weber

### **Synthesis of Semi-Insulating GaAs by As Implantation and Thermal Annealing: Structural and Electrical Properties**

Conf. on Ion Implantation

High dose As implantation in GaAs followed by annealing at 600° C results in the formation of semi-insulating GaAs layers. These layers are relaxed with an homogeneous distribution of metallic As precipitates similarly to what is observed in GaAs grown by molecular beam epitaxy at about 200° C (LT-MBE-GaAs), after annealing at 600° C. By selecting the implantation parameters it is possible to adjust the thickness of the subsequent SI layer and to monitor the amount of excess As in the crystal. By selecting the annealing temperature it is possible to fabricate either a material very similar to the As-grown LT-MBE-GaAs or a material similar to annealed LT-MBE-GaAs.

---

37464

A

No

K.M. Krishnan

### **Anisotropy, Transport Properties and Microstructures in Magnetic Thin Films and Nanostructures**

IV ICAM (submitted)

Atomically engineered metallic nanostructures and thin films offer new opportunities to elucidate the physics of magnetism, test new theories, and most importantly, build new materials with new and unique bulk properties. The wide range of experimental measurements possible in an electron microscopy environment, i.e. imaging, diffraction and spectroscopy, offers the possibility of the evaluation of the microstructure (physical, chemical and magnetic) at an appropriate length scale to interpret the unique properties exhibited by these materials. In this talk, I will introduce details of such electron-optical measurements and illustrate their applications with a number of examples, and address the following issues: perpendicular anisotropy in Co/Pt multilayers, and newly synthesized  $Mn_xGa_{1-x}$  epitaxial films on GaAs; the microstructure of phase separated granular alloys (Co/Ag) and permalloy/Au multilayers exhibiting giant magnetoresistance; and the correlation between the electron structure and enhanced saturation moment in Co-Cr thin films. In the latter system, quantitative correlations between microstructure and micromagnetics will also be discussed.

## Microstructurally Tailored Magnetic Thin Films and Nanostructures for New Technologies

Mag. Mats. & Devices Conf.

This is an ongoing program involving a dynamic iteration between forefront efforts in synthesis, characterization and control of microstructures to atomically engineer magnetic thin films with novel anisotropy, transport and hysteretic properties.

---

35851

A

No

F.M. Ross and R.R. Kola

## Dynamic Observations of the $\alpha$ - $\beta$ Phase Transformation in Thin W Films

MRS

Real-time TEM observations can be used to obtain quantitative information on thermodynamic parameters associated with phase transformations. We have used *in situ* techniques to examine the transformation from the metastable  $\beta$  phase of tungsten (A15 structure) to the stable  $\alpha$  (bcc) phase. Sputtered tungsten films, similar to those used in x-ray masks, are deposited directly onto electron transparent membranes. These specimens can then be examined and heated in the microscope, avoiding problems associated with specimen preparation artifacts or stress relaxation at free edges. A suitable choice of the sputtering conditions results in the growth of films with a well-controlled stress state, mainly comprised of the  $\beta$  phase. Analysis of video frames recorded at different temperatures allows us to visualise the progress of the transformation and derive parameters such as the activation energy. We have combined this information with atomic resolution imaging of the film structure, particularly the morphology of the voids. In this paper we will show how, for these films, the final void morphology is determined by the transformation from the metastable precursor phase. We will also characterise this phase transformation as a function of film thickness and stress state, and use the analysis to separate the effects of stress and surface and bulk diffusion in the transformation.

---

**Novel Phases in the Oxidation of  $\gamma$ -Titanium Aluminum**Acta Met et Mat. 42 4 1373 1994

This paper concentrates on the high temperature oxidation of  $\gamma$ -titanium aluminum. Samples of Ti-47.5 at % Al were subjected to a 1000° C oxygen environment for various times and subsequently examined by Auger Electron Spectroscopy (AES), X-ray Diffraction (XRD), Scanning Electron Microscopy (SEM), and optical microscopy. AES proved to be useful in identifying oxygen scavenging by  $\text{Ti}_3\text{Al}$  and also in examining a subscale Al depletion layer, which was found to contain two previously unreported phases, tentatively identified as  $\text{Ti}_{10}\text{Al}_6\text{O}$  and  $\text{Ti}_{10}\text{Al}_6\text{O}_2$ . These phases enabled an updated description of  $\gamma$ -titanium aluminum oxidation at temperatures from room temperature to above 1100°C.

**Microstructure of Silicon Nitride Ceramics Sintered with Rare-Earth Oxides**Acta Met. et Mat. 43 3 923 1995

Microstructures of  $\text{Si}_3\text{N}_4$  with crystallized grain boundaries of rare-earth silicates were investigated.  $\beta$ - $\text{Si}_3\text{N}_4$  grains in samples sintered with  $\text{Yb}_2\text{O}_3$  were more elongated than those sintered with  $\text{Dy}_2\text{O}_3$ . Amorphous thin layers between crystallized grain boundaries of silicate and  $\text{Si}_3\text{N}_4$  grains were recognized for both specimens sintered with  $\text{Dy}_2\text{O}_3$  and with  $\text{Yb}_2\text{O}_3$ . In the sample sintered with  $\text{Dy}_2\text{O}_3$ , very clean grain boundaries between  $\text{Si}_3\text{N}_4$  grains which did not contain the heavy elements were frequently recognized, while samples with  $\text{Yb}_2\text{O}_3$  had an amorphous grain boundary phase containing Yb. Unusual structures with distorted lattice images in regions rich in Si and O were discovered in crystalline Dy-silicate phases.

un-numbered                      M                      No  
P.M. Vasconcelos, H.-R. Wenk and C. Echer

### **In-situ Study of the Thermal Behavior of Cryptomelane by High-Voltage and Analytical Electron Microscopy**

Amer. Mineralogist    79 81 1994

Scanning electron microscope (SEM) and transmission electron microscope (TEM) studies show that cryptomelane and Cu-rich cryptomelane crystals from weathering profiles in Brazil range from 10 to 200 nm in diameter and have aspect ratios of 1:10 to 1:100 between the long and short dimensions. Acicular crystals identified in hand specimen and in the scanning electron microscope are often composed of bundles of fibers elongated along the c axis (tetragonal) or the b axis (monoclinic). *In-situ* heating with a high-voltage transmission electron microscope (HVEM) and an analytical electron microscope (AEM) indicates that upon heating in vacuum cryptomelane crystals begin to transform into a mixed hausmannite and manganosite phase at 648° C, and manganosite begins to form at 620° C. Cu-rich cryptomelane also loses K and exsolves native copper upon heating, suggesting that Cu occupies the same site (the A site) as K. Similar mineral transformations are observed when the same samples are heated in air, although the transformations occur at higher temperatures than those observed in vacuum.

---

35116                                      M                                      R  
D. Loretto, F.M. Ross, C.A. Lucas and G.C.L. Wong

### **Direct Observation of Interface and Surface Steps in Epitaxial Films by Dark-Field Transmission Electron Microscopy**

Appl. Phys. Letts.    65 14 1766 1994

We have used dark-field transmission electron microscopy to investigate <5 nm thick CaF<sub>2</sub> films grown on Si(111) by molecular beam epitaxy. Images formed with CaF<sub>2</sub>[111] reflections exhibit contrast at 1/3[111] high steps at the CaF<sub>2</sub> surface and at the CaF<sub>2</sub>/Si interface over large (>100 μm<sup>2</sup>), statistically significant areas. Direct evidence for step flow growth in CaF<sub>2</sub> has been obtained.

### Microstructure and Epitaxy of c-axis Oriented Single Crystal Cobalt Films Grown on Rigid Underlayers

Appl. Phys. Letts. 64 12 1499 1994

We have established the conditions to grow c-axis oriented Co Films on mica substrates and characterized their crystallography and microstructure in detail. In particular, these films are single crystal, c-axis oriented, Co<sub>hcp</sub> and are grown epitaxially by e-beam evaporation on either Ti or Ru underlayers.

### Epitaxial Lateral Overgrowth of Silicon by Chemical Vapor Deposition on Ultrathin Oxide Layers

Appl. Phys. Letts. 65 9 1142 1994

Selective epitaxial growth followed by epitaxial lateral overgrowth (ELO) of silicon through windows in SiO<sub>2</sub> in a hot-wall low-pressure chemical vapor deposition system has been used to fabricate silicon-on-insulator (SOI) structures. By careful *ex situ* and *in situ* surface cleaning and low-temperature processing, 2.5- $\mu$ m-thick, single-crystal silicon films have been successfully deposited over oxide layers as thin as 35Å. Dislocation densities in these SOI films over thin oxides are higher than those found in SOI films deposited on thicker oxides. Nucleation of dislocations in the epitaxially grown film is attributed to pinhole expansion in the ultrathin oxide layers during *ex situ* cleaning, prebake treatment, or ELO processing. An unusual crystallographic defect with attributes of a microtwin-stacking fault complex are also observed in the ELO film appearing over thin oxide layers. A model is proposed to explain this class of defect structure and its formation mechanism.

**Rapid Thermal Annealing of Low-Temperature GaAs Layers**Appl. Phys. Letts. 66 16 1 1995

Electron microscopy studies of annealed GaAs layers grown by molecular beam epitaxy at low temperature (200° C) were used to monitor growth of As precipitates. Oswald ripening kinetics was used to deduce a migration enthalpy of  $1.4 \pm 0.3$  eV for the diffusion mediating defect. A conclusion picture of the dominant diffusion mechanism can be given, attributing this value to the migration enthalpy of gallium vacancies ( $V_{Ga}$ ), which is well established by other experiments. The present studies indicate that growth of As precipitates is driven by supersaturation of  $V_{Ga}$ .

---

un-numbered

M

R

X.W. Lin, J. Washburn, Z. Liliental-Weber, A. Sasaki, A. Wakahara and Y. Nabetani

**Morphological Transition of InAs Islands on GaAs (001) Upon Deposition of a GaAs Capping Layer**Appl. Phys. Letts. 65 13 1677 1994

The interaction between a GaAs cap and InAs islands grown on vicinal GaAs(001) has been studied by transmission electron microscopy and atomic force microscopy. Samples were prepared by molecular beam epitaxy at 480° C. Upon GaAs cap deposition, it was found that the previously grown InAs islands undergo a novel type of morphological transition, i.e., a transition from disk-shaped to ring-shaped islands. InAs becomes depleted or entirely absent in the central area of what had been a disk-shaped InAs island. The GaAs cap was also shown to be virtually absent within the same central region, resulting in the formation of crater-like surface depressions.

un-numbered                      M                      No

Y. Chen, X. Liu, E. Weber, E.D. Bourret, Z. Liliental-Weber, E.E. Haller, J. Washburn, D.J. Olego, D.R. Dorman et al.

### **Structures and Electronic Properties of Misfit Dislocations in ZnSe/GaAs(001) Heterojunctions**

Appl. Phys. Letts.    65 5 549 1994

Studies of the structure and electrical properties of regular and irregular misfit dislocations in undoped and N-doped ZnSe epilayers grown on GaAs(001) substrates by transmission electron microscopy (TEM), and cathodoluminescence (CL), are reported. In undoped ZnSe epilayers, two sets of misfit dislocation arrays were observed: a straight orthogonal array along [110] and [110], and an irregular array roughly along [100] and [010] directions. The CL observations suggest that the irregular dislocations trap carriers more efficiently than the dislocations along  $\langle 110 \rangle$ , possibly due to the high density of kinks existing along the zig-zag irregular dislocations. These irregular dislocations can be eliminated by doping nitrogen in the ZnSe epilayer with  $[N] > 1 \times 10^{18} \text{ cm}^{-3}$ .

---

36236                                      M                                      R

B.M. Simion, G. Thomas, R. Ramesh, V.G. Keramidas and R.L. Pfeffer

### **Growth and Characterization of $(\text{Y}_3\text{Fe}_5\text{O}_{12}\text{-Bi}_3\text{Fe}_5\text{O}_{12})$ Heterostructures by Pulsed Laser Deposition**

Appl. Phys. Letts.    66 7 830 1995

Superlattice heterostructures consisting of alternating single crystalline ferrimagnetic yttrium-iron-garnet (YIG) and bismuth-iron-garnet (BIG) thin film layers on gadolinium-gallium-garnet substances shown an increased saturation magnetization with respect to that of the monolayered structures grown under the same conditions. The observed effect is attributed to the distortions introduced in the YIG layers by the adjacent BIG layers. In this letter, we report our growth approach, by pulsed laser deposition, of these unusually performing thin films heterostructures.

### **Nucleation of Misfit Dislocations in $\text{In}_{0.2}\text{Ga}_{0.8}\text{As}$ Epilayers Grown on GaAs Substrates**

Appl. Phys. Letts. B 66 4 499 1995

Misfit dislocation arrays in  $\text{In}_{0.2}\text{Ga}_{0.8}\text{As}$  epilayers grown on GaAs substrates tilted  $2^\circ$ - $10^\circ$  away from exact (001) toward varied directions have been studied by transmission electron microscopy. A method has been developed to determine the glide plane and the Burgers vector of each misfit dislocation in the tilted InGaAs/GaAs interfaces. Based on experimental observations and theoretical analyses, it is proposed that a stacking fault surrounded by a  $30^\circ$  partial is at first generated by a growth error, followed by thermally activated nucleation of a  $90^\circ$  partial dislocation that removes the stacking fault and forms a  $60^\circ$  dislocation. From the frequency of nucleation events versus the dislocation glide force, the energy barrier for dislocation nucleation of  $\alpha$  and  $\beta$   $90^\circ$  partial dislocations was determined to be equal to 1.5 and 1.4 eV respectively.

---

37029

M

No

K.M. Krishnan

### **Enhanced Saturation Magnetization, Electronic Structure and Compositional Segregation in Epitaxially Grown Co-Cr Thin Films**

Appl. Phys. Letts. (submitted)

We have used the recently established linear correlation between the total intensities of the  $L_{3,2}$  "white lines" in electron energy-loss spectroscopy and the number of unoccupied 3d states to probe the local electronic structure in epitaxially grown Co-Cr thin films. The significant enhancement of saturation magnetization measured for these epitaxial films, when compared to homogenized bulk alloys, has been correlated directly to the unoccupied 3d states local to the Co atoms in these materials. These measurements are the first direct electronic structure evidence that may support models associating the enhancement of saturation magnetization with intragranular segregation in Co-Cr thin films.

**Solid-State Reaction in Pd/ZnSe Thin Film Contacts**

Appl. Phys. Letts. (submitted)

We report on solid-state reactions in Pd thin film contacts on ZnSe at temperatures below 500° C. We found that a solid-state reaction was initiated at the Pd/ZnSe interface by annealing at 200° C. A tetragonal ternary phase, Pd<sub>5</sub>ZnSe, consisting of highly oriented grains was formed as a result of this reaction. This phase was found to be stable up to an annealing temperature of 400° C. The crystallography and morphology of this ternary Pd-ZnSe phase was studied by x-ray diffraction and transmission electron microscopy; it has similarities to the analogous ternary Pd-GaAs phase formed in the Pd/GaAs contact structure. The Pd/ZnSe interface was found to be thermally more stable than the corresponding Pd/GaAs and Pd/Si structures. Comparisons are made between Pd/semiconductor interfacial phenomena on the three semiconductors.

 **$\alpha$  to  $\beta$  Transformation and Microstructural Changes of Si<sub>3</sub>N<sub>4</sub> During Sintering**

Ceramic Transactions 42 157 1994

Changes of density, the  $\alpha$ - $\beta$  phase transformation, and composition of grains and grain-boundaries during sintering of Si<sub>3</sub>N<sub>4</sub> with various sintering conditions using additives of Y<sub>2</sub>O<sub>3</sub> and Al<sub>2</sub>O<sub>3</sub> were investigated. The phase determination of individual Si<sub>3</sub>N<sub>4</sub> grains was performed by convergent beam electron diffraction (CBED). The relations between densification and transformation were divided into two groups, depending on the additive compositions. Al dissolution into Si<sub>3</sub>N<sub>4</sub> grains occurred mostly during the  $\alpha$ - $\beta$  transformation process. The concentration of Al and O in the grain boundaries decreased as the  $\alpha$  to  $\beta$  transformation progressed.

### **Quantitative Analysis of Atomic Displacements in HRTEM Images**

Comp. Ass't. Micros. 6 3 129 1994

In images of imperfect crystals it is important to determine the positions of atoms away from the perfect lattice positions. Although atoms are not always individually resolved, there are many systems where atoms are imaged as either white or black "dots". In these systems, the localization of atoms is made by searching for peaks in the image. However, practical problems are often encountered using peak finding algorithms found in available software packages. This paper describes a method for quantifying the atomic displacements in High Resolution TEM images to high accuracy. The method treats common problems associated with intensity saturation, noise and spurious peaks. The method has been applied to a HRTEM image of a modulated structure,  $\text{Ti}_{50}\text{Pd}_{42}\text{Cr}_8$  where the atoms are displaced from the perfect lattice sites by a "frozen" displacement wave. In addition to describing the peak finding algorithm and the refinement of peak positions to sub-pixel accuracy, the paper also shows how spurious peaks can be eliminated and how missing peaks can be reintroduced.

---

un-numbered

M

R

L.T. Wille, J.L. Rogers, C.P. Burmester and R. Gronsky

### **Towards First Principles Theories of Materials and Biological Systems: The Need for Massive Parallelism**

Future Gen. Com. Syst. 10 331 1994

The first-principles paradigm, i.e., the calculation of a physical, chemical or biological system's properties without including any fitted or adjustable parameters, is one of the most powerful in the scientist's quest to understand nature. Unfortunately, most first-principles computations involve quite complicated governing equations and large system sizes, both of which have a detrimental effect on memory size and computer time requirements. Using two relatively simple yet realistic models, one in materials science and one in biophysics, it is discussed here how massive parallelism can make such studies feasible.

### **HREM Analysis of Structure and Defects in a $\Sigma 5$ (210) Grain Boundary in Rutile**

Interface Sci. **2** 125 1994

The structure of a  $\Sigma 5$  (210) boundary in rutile was investigated by high resolution electron microscopy (HREM). The boundary was stepped with an average inclination of about  $5^\circ$  from the symmetrical (210) plane. The steps were associated with  $1/5[210]$  DSC lattice dislocations accommodating a deviation of about  $2^\circ$  from the exact  $\Sigma 5$  misorientation of  $53.1^\circ$ , and resulting in a misorientation of  $51^\circ$ . The boundary topography, the location of structural units and the local symmetry were determined using pattern recognition techniques. Flat terraces between steps had a periodic  $\Sigma 5$  (210) structure which exhibited mirror glide symmetry. Image simulations showed best agreement with experimental images for a model structure with a rigid body shift of 0.21nm parallel, and a 0.10nm volume contraction normal to the interface. This structure requires a high density of defects or an excess of Ti ions, presumably of lower oxidation state.

---

un-numbered

A

R

T. Mitchell, Jr., L.C. De Jonghe, W.J. Moberly-Chan and R.O. Ritchie

### **Silicon Carbide Platelet/Silicon Carbide Composites**

J. Amer. Cer. Soc. **78** 1 97 1995

Alpha-silicon carbide platelet/beta-silicon carbide composites have been produced in which the individual platelets were coated with an aluminum oxide layer. Hot pressed composites showed a fracture toughness as high as  $7.2 \text{ Mpa.m}^{1/2}$ . The experiments indicated that the significant increase in fracture toughness is mainly the result of crack deflection and accompanying platelet pull out. The coating on the platelets also served to prevent the platelets from acting as nucleation sites for the alpha to beta phase transformation, so that advantageous microstructure remains preserved during high temperature processing.

### **Giant Magnetoresistance and Microstructural Characteristics of Epitaxial FeAg and CoAg Granular Thin Films**

J. Appl. Phys. 75 10 6900 1994

Giant magnetoresistance (GMR) and its relationship with the microstructure in phase separated FeAg and CoAg granular thin films grown epitaxially on (001) NaCl substrates by MBE, were studied by transmission electron microscopy (TEM) and magnetic characterization techniques. The influence of microstructural features such as growth twins, Fe and Co phase distribution, grain size distribution and orientation on the observed magnetic properties of these granular alloy films will be discussed.

---

35176

No

A

X.W. Lin, J. Washburn, Z. Liliental-Weber and H. Bernas

### **Coarsening and Phase Transition of FeSi<sub>2</sub> Precipitates in Si**

J. Appl. Phys. 75 9 4686 1994

FeSi<sub>2</sub> precipitates were produced in Si(001) wafers by an ion-beam induced epitaxial crystallization process and subsequently annealed at temperatures in the range 650-900° C. The resulting precipitate coarsening and phase transition were studied by transmission electron microscopy. The coarsening process basically involves the evolution of plate-shaped precipitates. The lengthening rate of the precipitates is considerably greater than the thickening rate, because the two broad faces of a plate are coherent or semicoherent, while the plate edges are incoherent. The lengthening kinetics was shown to be volume-diffusion controlled and obey a cube power law. The corresponding activation energy was determined to be 3.55 eV, in excellent agreement with the value predicted by the classical Ostwald ripening model. In contrast, we demonstrated that the thickening process is interface controlled, which involves the migration of the interfaces via a ledge mechanism. Accordingly, an apparent activation energy of 2.18 eV was obtained. The precipitate coarsening is accompanied by phase transitions. Upon annealing at 650 ° C, it was observed that  $\gamma$ -FeSi<sub>2</sub> precipitates tend to transform from a fully aligned (A-type) to a twinned (B-type) orientation with respect to the Si matrix. The observations suggest that the phase transition of FeSi<sub>2</sub> is size dependent.

---

### **Change of Structure and Location of Misfit Dislocations in $\text{In}_x\text{Ga}_{1-x}\text{As}/\text{GaAs}$ (001) System**

J. Appl. Phys. (submitted)

The structure and locations of misfit dislocations have been investigated experimentally and theoretically in different strained  $\text{In}_x\text{Ga}_{1-x}\text{As}$  ( $0.2 \leq x \leq 1$ ) epilayers grown on GaAs substrates. The misfit dislocations in the  $\text{In}_{0.2}\text{Ga}_{0.8}\text{As}$  epilayers were predominantly dissociated  $60^\circ$  dislocations with the  $90^\circ$  partials lying in the interface and the  $30^\circ$  partials pushed into the substrate. In  $\text{In}_{0.3}\text{Ga}_{0.7}\text{As}$  epilayers, misfit dislocations of both  $60^\circ$  and  $90^\circ$  types were present either in undissociated form or split into partials. These dislocations were not all near the interface; some were scattered through the epilayer. The presence of dislocations of  $60^\circ$  type located away from the interface for intermediate misfits is rationalized by considering the balance of forces acting on these dislocations. In  $\text{In}_{0.4}\text{Ga}_{0.6}\text{As}$  and in InAs epilayers, misfit strain was accommodated almost entirely by  $90^\circ$  undissociated dislocations. A model is proposed for the formation of  $90^\circ$  edge dislocations to explain the transition of dominant misfit dislocation type from  $60^\circ$  to  $90^\circ$  type with increasing mismatch.

---

35150

M

No

T. Komaya, A.T. Bell, Z. Weng-Sieh, R. Gronsby, F. Engelke, T.S. King and M. Pruski

### **The Influence of Metal-Support Interactions on the Accurate Determination of Ru Dispersion for $\text{Ru}/\text{TiO}_2$**

J. Catalysis 149 142 1994

Titania-supported Ru catalysts have been characterized by TEM,  $^1\text{H}$  NMR, and  $\text{H}_2$  chemisorption to determine the metal particle size, the fraction of the metal surface available for  $\text{H}_2$  chemisorption, and the  $\text{H}_2$  adsorption capacity of the catalyst, as functions of the reduction temperature. TEM micrographs show that as the reduction temperature rises from 573 K to 773 K the average particle size of Ru remains the same but the surface of the particles is covered to an increasing extent by an amorphous layer of titania. Quantitative estimates of the fraction of the Ru particle surface available for  $\text{H}_2$  chemisorption were obtained by  $^1\text{H}$  NMR. The NMR spectra also show that a fraction of the adsorbed  $\text{H}_2$  spills over onto the support and that as a consequence measurements of total  $\text{H}_2$  chemisorption overestimate the number of Ru sites available for  $\text{H}_2$  adsorption. The implications of these results for the correct calculation of Ru dispersion and the determination of turnover frequencies for reactions carried out over  $\text{Ru}/\text{TiO}_2$  are discussed.

T. Komaya, A.T. Bell, Z. Weng-Sieh, R. Gronsky, F. Engelke, T.S. King and M. Pruski

**Effects of Dispersion and Metal-Metal Oxide Interactions on Fischer-Tropsch Synthesis over Ru/TiO<sub>2</sub> and TiO<sub>2</sub>-Promoted Ru/SiO<sub>2</sub>**

J. Catalysis 150 400 1994

The activity of Ru/TiO<sub>2</sub> and TiO<sub>2</sub>-promoted Ru/SiO<sub>2</sub> catalysts for Fischer-Tropsch synthesis have been investigated. The Ru dispersion of these catalysts was determined by TEM and the fraction of the Ru surface available for H<sub>2</sub> adsorption was determined by <sup>1</sup>H NMR. Even after low-temperature reduction, the surface of titania-containing catalysts is covered by titania to a substantial degree. The specific activity and selectivity of these catalysts is dominated by the interactions occurring between the Ru particles and the titania overlayer. As the fraction of the Ru particle surface covered by titania increases, the turnover frequency for CO consumption passes through a maximum, while that for methane formation decreases monotonically. The probability for chain growth and the olefin to paraffin ratio of the products increase with increasing titania coverage. These trends are attributed to the effects of the titania overlayer on the catalytic properties of Ru.

---

36167

M

P

V. Radmilovic, H. Gasteiger and P.N. Ross

**Structure and Chemical Composition of a Supported Pt-Ru Electrocatalyst for Methanol Oxidation**

J. Catalysis 154 98 1995

High resolution electron microscopy (HREM) and x-ray microchemical analysis (EDS) were used to characterize composition, size, distribution and morphology of Pt-Ru particles with nominal Pt:Ru ratio 1:3 and 3:1, supported on carbon black. The particles are predominantly single nanocrystals with diameters in the order of 2.0 to 2.5 nm. Occasionally, twinned particles are also observed. All investigated particles represent solid solutions of Pt and Ru with compositions very close to the nominal one. Based on two-dimensional projection in high resolution images, it is suggested that the well resolved particles are of cubo-octahedral shape. In addition to {200} and {111} facets, {113} facets are also observed.

### Microstructure of Sputtered Epitaxial $\text{Ni}_{0.80}\text{Fe}_{0.20}/\text{Ni}_x\text{Co}_{1-x}\text{O}$ Exchange Coupled Bilayers on $\alpha\text{-Al}_2\text{O}_3$ (0001)

J. Electronic Mats. **23** 10 1994

Epitaxial  $\text{Ni}_{0.80}\text{Fe}_{0.20}/\text{Ni}_x\text{Co}_{1-x}\text{O}$  bilayers have been grown on  $\alpha\text{-Al}_2\text{O}_3$  (0001) substrates by dc-sputtering. X-ray diffraction and transmission electron microscopy have been employed to characterize these exchange-coupled films. The x-ray diffraction spectrum shows only the (111) family of peaks in both  $\text{Ni}_{0.80}\text{Fe}_{0.20}$  and  $\text{Ni}_x\text{Co}_{1-x}\text{O}$  films. Growth orientation relationships have been determined from diffraction patterns taken in planar view and cross section. The relationships are:  $(111)\text{Ni}_{0.80}\text{Fe}_{0.20} // (111)\text{Ni}_x\text{Co}_{1-x}\text{O} // (0001)\alpha\text{-Al}_2\text{O}_3$  and  $[110]\text{Ni}_{0.80}\text{Fe}_{0.20} // [110]\text{Ni}_x\text{Co}_{1-x}\text{O} // [1100]\alpha\text{-Al}_2\text{O}_3$ . The microstructure of these films as well as the interfacial structure between  $\text{Ni}_{0.80}\text{Fe}_{0.20}$  and  $\text{Ni}_x\text{Co}_{1-x}\text{O}$  have been analyzed in high resolution electron microscopy and are described in this paper. In addition, the dependence of the exchange coupling field on interfacial roughness is discussed.

### Micromagnetics and Microstructure of Epitaxially Grown Co and Co-Cr Films Suitable for Perpendicular Magnetic Recording

J. Mag. Soc. of Japan **18** S-1 15 1994

Highly c-axis oriented, single crystal films of  $\text{Co}_{1-x}\text{Cr}_x$  ( $0 < x < 0.3$ ) have been grown epitaxially on mica substrates by e-beam evaporation. The orientation relationship is basically  $(00.1)_{\text{mica}} // (00.1)_{\text{Co}}$ , and  $(11.0)_{\text{mica}} // (10.0)_{\text{underlayer}} // (10.0)_{\text{Co}}$ . Films grown on Ru underlayers have an average grain size of 50-80nm, negligible fcc content and very narrow c-axis dispersion ( $\Delta\theta \sim 0.7\text{-}1.5^\circ$ ). For Co films ( $x=0$ ), the as-grown magnetization structure are mainly  $180^\circ$  domain walls with a uniform distribution of cross-ties for thinner samples ( $< 300 \text{ \AA}$ ), whilst thicker ( $> 400 \text{ \AA}$ ) ones show stripe domains. These images were analyzed in detail to measure the wall widths and associated energy densities for as-grown, remanent and ac-magnetized samples. As expected, the magnetic properties of these films are composition dependent. However, for any Cr concentrations, these films exhibit the largest saturation magnetization when compared with either sputtered or evaporated samples. This enhancement can be attributed to a nanometer-scale segregation of Cr, which in these samples, could be particularly aided by the diffusion of the close-packed planes of the films with very narrow c-axis dispersions. Preliminary x-ray microanalysis and NMR data support this interpretation.

35165

M

R

Z. Weng-Sieh, P. Krulevitch, R. Gronsky and G.C. Johnson

**Stress Induced Formation of Structural Defects on the {311}Planes of Silicon**

J. Mat. Res. 9 8 2057 1994

Structural defects occurring on the {311} planes of single crystal silicon have been observed near the bottom oxide corner in silicon-on-insulator structures formed by selective epitaxial growth. These {311} defects exhibit a preferential orientation and are clustered near the silicon/silicon dioxide interface. This new observation provides an opportunity to study the mechanism of {311} defect generation in a system with discernible microstructure and stress state. High resolution electron microscopy combined with analytical and numerical three-dimensional stress modeling are used to show the dependence of these defects on the local stress field, and to establish their origin in terms of the homogeneous dislocation nucleation model.

---

35934

M

No

X.Y. Song, W.-Q. Cao, M.R. Ayers and A.J. Hunt

**Carbon Nanostructure in Silica Aerogel Composites**

J. Mat. Res. 10 2 251 1995

In this letter we shall report a new method of preparing carbon nanotubes and their derivatives using silica aerogels as a matrix for the deposition of carbon. We shall present the observation of hollow graphite tubes and rings including nested structures in nanometer dimensions using high resolution transmission electron microscopy. Furthermore, we propose a model for the growth of carbon nanotubes in three steps including nucleation, growth and closure of tubes.

**Phase Transformation and Microstructural Changes of  $\text{Si}_3\text{N}_4$  During Sintering**J. Materials Science 30 2194 1995

Changes of density, the  $\alpha$ - $\beta$  phase transformation, and composition of grains and grain-boundaries during sintering of  $\text{Si}_3\text{N}_4$  with various sintering conditions using additives of  $\text{Y}_2\text{O}_3$  and  $\text{Al}_2\text{O}_3$  were investigated. The phase determination of individual  $\text{Si}_3\text{N}_4$  grains was performed by convergent beam electron diffraction (CBED). The relations between densification and transformation were divided into two groups, depending on the additive compositions. Al dissolution into  $\text{Si}_3\text{N}_4$  grains occurred mostly during the  $\alpha$ - $\beta$  transformation process. The concentration of Al and O in the grain boundaries decreased as the  $\alpha$  to  $\beta$  transformation progressed.

---

36210

M

R

A. Hütten and G. Thomas

**High Resolution Microscopy Characterization of Nanostructured Materials**J. Nanophase Materials 260 181 1994

High resolution microscopy techniques have been used to study fundamental problems related to the improvement of permanent magnets, to quantify interfacial roughness of layered structures, and to determine the decomposition behavior of heterogeneous alloys. The microstructural information obtained provides data for correlation with the relevant magnetic data and, hence, considerable insight into materials behavior, aiding in the understanding and improvement of materials performance.

### **In-Situ High-Resolution Electron Microscopy Observations of Nanometer-Size Pb Inclusions in Al**

J. of Microscopy (accepted)

Nanometer size Pb precipitates were produced by implantation of Pb ions at 40 keV into Al thin films at 150° C. Both Pb and Al are face centered cubic and the precipitates invariably adopted the cube-cube orientation relationship. The shape of most precipitates was close to a cubo-octahedron, faceted on eight [111] and six [100] interfaces. *In-situ* HREM observations of the precipitates were made near a  $\langle 110 \rangle$  common zone axis and the thermal behavior was recorded on video tape. The precipitates inside the grains remained solid up to ~30° C above the bulk melting point of lead (327° C). The melted precipitates remained as liquid inclusions due to the lack of solubility of lead in Al. Resolidification of the precipitates began to take place when the sample was cooled to around the bulk melting point of lead. Morphologies of the lead precipitates as well as atomic-scale changes associated with the melting and resolidification were recorded and analyzed on video and HREM micrographs.

---

un-numbered

M

No

J.B. Liu, M.L. Dass and R. Gronsky

### **Transmission Electron Microscopy Study of Two Dimensional Semiconductor Device Junction Delineation by Chemical Etching**

J. Vac. Sci. & Tech. **B-12** 1 353 1994

Quantitative chemical delineation of both n+ and p+ junctions in silicon-based integrated circuits has been achieved and monitored with respect to etching time, temperature, and ultraviolet illumination, using samples prepared by a new planar polishing technique for uniform initial flatness. Junction depths and dopant profiles obtained from cross-sectional transmission electron microscopy images are compared and cross-calibrated with both secondary ion mass spectrometry and spreading resistance profiling, confirming that dopant concentrations of  $10^{17} \text{ cm}^{-3}$  are detected and laterally mapped with better than 10 nm spatial resolution.

X.W. Lin, Z. Liliental-Weber, S. Nabetami, A. Wakahara, A. Sasaki, J. Washburn and E.R. Weber

### **Molecular Beam Epitaxy of InAs and its Interaction with a GaAs Overlayer on Vicinal GaAs (001) Substrates**

J. Vac. Sci. Tech. B 12 4 2562 1994

GaAs/InAs/GaAs heterostructures were grown by molecular beam epitaxy on vicinal GaAs (001) substrates. Effects of substrate misorientation on the early stage of InAs epitaxy, as well as the interaction between InAs and a GaAs overlayer, were studied by transmission and scanning electron microscopes and by photoluminescence measurements. The formation of InAs islands were observed after a few monolayer InAs deposition. Two major results were obtained in this study: (a) Upon deposition of a crystalline GaAs overlayer, InAs islands undergo a novel type of morphological transition, i.e., from disk-shaped to ring-shaped ones. (b) Substrate misorientation results in anisotropic effects on InAs island formation. In comparison with on-axis or [110] tilted samples, substrate misorientation toward [110] by up to 5° leads not only to reduction in InAs island density by a factor of 2, but also to the formation of InAs quantum dots. These results were found to be consistent with photoluminescence experiments.

---

35631 M R

Z. Liliental-Weber, P.V. Schwartz and J.C. Sturm

### **Structure of Oxygen-Doped Silicon Grown by Chemical Vapor Deposition at Low Temperature**

J. Vac. Sci. Tech. B 12 4 2511 1994

The relation between the structural quality of Si:O layers grown by chemical vapor deposition at low temperatures (700-750° C) and electrical properties was determined, using TEM, SIMS, and resistivity measurements. Oxygen concentration was in the range of  $6 \times 10^{-19}$  -  $6 \times 10^{-20}$  cm<sup>-3</sup>. Amorphous SiO<sub>x</sub> precipitates formed at the lower interface (between the Si buffer and Si:O layer) when silane was used. Smaller precipitates were distributed through the layer. In layers with higher oxygen concentration, the high density of stacking faults originated at the interface and propagated through the layer. The Si capping layer grown on top of Si:O had a density of stacking faults two orders of magnitude lower. For lower oxygen concentration, stacking faults were not formed and the size of precipitates was smaller. Resistivity of  $\sim 10^5$  and  $\sim 10^6$  Ω cm was measured in the layers with lower and higher oxygen content, respectively. Only for the Si:O layers grown in the same range of temperatures (700° C) using dichlorosilane oxygen-induced stacking faults were formed at the upper interface (between Si:O and the capping layer). Some small precipitates were formed at the lower interface, but no visible precipitates were present in the Si:O layer. These layers were not semi-insulating. It was concluded that the mechanism to explain semi-insulating properties might be related to the presence of the SiO<sub>x</sub> precipitates.

---

un-numbered                      M                      No

X.W. Lin, W.V. Lampert, T.W. Haas, P.H. Holloway, Z. Liliental-Weber, W. Swider and J. Washburn

### **Metallurgy of Al-Ni-Ge Ohmic Contact Formation on n-GaAs**

J. Vac. Sci. Tech. B (in press)

Al-Ni-Ge ohmic contacts on n-GaAs were prepared by sequential vapor deposition and subsequently annealed by 500° C. The metallurgical properties of the contacts were studied by transmission electron microscopy. It was found that while Al-Ni-Ge as a whole is stable against GaAs, extensive interfacial reactions readily occur within the contact layers, resulting in a very stable layered structure of the type  $\text{Al}_3\text{Ni}/\text{Ni-Ge}/\text{GaAs}$ , with  $\epsilon\text{-Ni}_3\text{Ge}_3$  being the major phase in the Ni-Ge layer. GaAs twins and Ni-As precipitates were found in a thin layer immediately below the metallization, suggesting that the ohmic behavior can be accounted for, in terms of a GaAs regrowth mechanism.

---

un-numbered                      M                      No

X.W. Lin, Z. Liliental-Weber, J. Washburn, E.R. Weber, A. Sasaki, A. Wakahara and T. Hasegawa

### **Ge/Si Heterostructures Grown by Sn Surfactant-Mediated Molecular Beam Epitaxy**

J. Vac. Sci. Techn. B (in press)

Ge/Si heterostructures were grown on Si (001) by Sn-submonolayer-mediated molecular beam epitaxy (MBE) and characterized by a variety of techniques, in order to study the behavior of Sn surfactant during Ge and Si growth and its influence on Ge/Si interface quality. It was found that Sn strongly segregates to the growing surface of both Ge and Si and that the presence of Sn surfactant can effectively suppress Ge segregation into a Si overlayer and enhance the surface mobility of adatoms. These results suggest that Sn-mediated epitaxy can be used as a viable method to produce Ge/Si superlattices, with an interface quality superior to those grown either by conventional MBE or with other types of surfactants.

**Electron Microscopy Characterization of GaN Grown by MBE on Sapphire and SiC**

J. Vac. Sci. Techn. B (in press)

Transmission electron microscopy was used for the characterization of GaN epitaxial layers grown by molecular beam epitaxy on two different substrates: sapphire ( $\text{Al}_2\text{O}_3$ ) and 6H-SiC. GaN layers grown on both substrates crystallize with the wurtzite structure. Despite the very different lattice mismatch associated with their two substrates, similar types of defects were formed in the GaN layer, only their density differed. In addition to small angle sub-grain boundaries, two other types of defects were seen in cross-sectioned samples: defects parallel to the growth surface and microtwins with a width of about 8-10 nm perpendicular to the growth surface. The parallel defects were identified as stacking faults leading to local fcc atom arrangement in the layer and are believed to be growth defects. The density of these faults decreased with layer thickness. However, the density of the vertical microtwins remained constant through the layer. Slight local lattice twist between the microtwin and surrounding areas or differences of stoichiometry are suggested as an explanation for the observed contrast of the high resolution images.

**A Comparison Between Three Simple Crystallographic Principles of Precipitate Morphology**Met. Trans. A 25A 9 1857 1994

The connection between the optimum shape and orientation relationship of precipitates in a solid is examined. Three simple criteria for precipitate morphology are compared and illustrated schematically: the principle that precipitate dimensions tend to be inverse to the magnitude of the transformation strain; the postulate that precipitates are bounded by unrotated planes (eigenplanes); and the proposal that interfaces are parallel to the planes of three independent dislocation loop arrays necessary to accommodate the transformation strain completely. These principles are illustrated for different orientation relationships and it is shown that special features are displayed by invariant line precipitates. The implications of these criteria for experimental studies of precipitate morphologies are discussed and their predictions compared with results from a recent study of lath-shaped precipitates in Cu-Cr alloys.

### **Studies on Ordered Mesoporous Materials III: Comparison of MCM-41 to Mesoporous Materials Derived from Kanemite**

Micropor. Mats. 4 1 1995

MCM-41 and mesoporous materials derived from kanemite are synthesized and characterized by x-ray powder diffraction (XRD), N<sub>2</sub> adsorption/desorption, cyclohexane and water physical adsorption, scanning electron microscopy (SEM), transmission electron microscopy (TEM), thermogravimetric analyses (TGA, FTIR and <sup>13</sup>C and <sup>29</sup>Si MAS NMR spectroscopy. Both preparations yield mesoporous materials with narrow pore size distributions and somewhat similar physicochemical properties. However, due to a higher degree of condensation in the silicate walls of the materials derived from kanemite, these samples have higher thermal and hydrothermal stability than MCM-41. Additionally, the mechanisms by which these two types of materials are formed are dramatically different.

### **Preparation of Oxide Superconductor Specimens for TEM Examination**

Micros. Res. & Techn. 30 2 167 1995

We have investigated a wide variety of oxide superconductors, and report here on a number of techniques that can be effectively used to prepare TEM specimens from these materials. Crushing, cleaving, ion milling, ultramicrotomy, and jet polishing all were successfully utilized, and details of each technique, as well as equipment used, are described. Selection among these methods depends both on the starting form of the material and on the information required. Ion milling and crushing generally give the best results and have the widest applicability in our particular work, while crushing and cleaving involve the least equipment cost. In some cases, particularly with ion milling and jet polishing, small variations in the details of preparation have a dramatic effect on the success rate. We have found it to be a great advantage that the same techniques can be applied in a similar manner to a whole range of oxide materials, even (with some refinements and special precautions) to those which are extremely oxygen or moisture sensitive.

### A Method for Jet Polishing Two-Phase Materials

Micros. Res. & Techn. (submitted)

A two-phase jet polishing technique is described, which, utilizing the effects of the characteristic current-voltage behavior of electropolishing solutions, can produce excellent TEM foils of relatively coarse two-phase materials.

---

35332

M

R

U. Dahmen

### Evolution of Ge Precipitate Morphology in Al

MRS Bulletin 19 6 22 1994

*In-situ* high voltage electron microscopy has been employed to study shape transformations of Ge precipitates in an Al-Ge alloy. During temperature cycling, lath-shaped Ge precipitates with a low-symmetry orientation relationship dissolved and regrew at their ends, becoming rounded during dissolution and sharply faceted during regrowth. These observations illustrate the strong dependence of growth mechanism and kinetics on the interface structure and are discussed in terms of a roughening transformation similar to that known for solid surfaces. These mechanisms have strong implications for the control of precipitate morphologies and the stability of interfaces in device structures.

## Materials Science in the Electron Microscope

MRS Bulletin 19 6 17 1994

Techniques which combine real time image acquisition with high spatial resolution have contributed to our understanding of a remarkably diverse range of physical phenomena. In this issue of MRS Bulletin we will present recent advances in materials science which have been made using the techniques of transmission electron microscopy (TEM), including holography, scanning electron microscopy (SEM), low energy electron microscopy (LEEM), and high voltage electron microscopy (HVEM).

---

un-numbered

M

R

R.D. Twisten, J.M. Gibson and F.M. Ross

## Visualization of Dynamic Near Surface Processes

MRS Bulletin 19 6 38 1994

Electron microscopy has played an undeniably important role in the development and understanding of new materials. One particular method, plan-view transmission electron microscopy (TEM), has been used to reveal many aspects of materials and to help answer questions that are not accessible by other methods. In plan-view TEM, materials are studied either by the image contrast caused by diffraction or by direct diffraction analysis. The studies are often at a somewhat lower resolution than is possible with some other electron-based microscopies or, in the case of diffraction, must be interpreted in terms of an average effect. Nevertheless, plan-view TEM is very useful because properties at these intermediate length scales typically determine important materials characteristics. It is plan-view microscopy that gives us the big picture of what is happening in a material. Until recently, TEM studies of materials have entailed comparing samples taken at various stages of processing and trying to observe and understand the mechanisms that determine the material behavior. With the advent of controllable specimen environments, materials processing has been taken into the TEM, allowing direct observation of the microstructural development. Here we will focus particularly on surface and near-surface processes, such as oxidation.

---

## High Resolution Electron Microscopy of Interfaces

MSA Bulletin 24 1 341 1994

This paper reviews recent progress in high resolution electron microscopy (HREM) of internal interfaces in solids. A brief summary of generic interface features of interest is followed by specific examples of HREM investigations of grain boundaries and heterophase interfaces. Features of interest include interface roughness, rigid body displacements, faceting, steps or ledges, elastic displacement fields, atomic bonding, composition gradients and localized atomic relaxation into structural units. Two types of analysis, direct interpretation and comparison with image simulations are applicable to different types of interface characteristics. Critical issues of current importance and recent developments in technique are outlined for asymmetrical and symmetrical grain boundaries and for metal-semiconductor and metal-ceramic interfaces.

---

37079

M

No

K.M. Krishnan, N. Thangaraj, R.F.C. Farrow, R.F. Marks, A. Cebollada and S.S.P. Parkin

## Atomic Roughening and Local Alloying Dwarf Giant Magnetoresistance in Metallic Multilayers

Nature

Since their recent discovery, inter-layer coupling and the associated giant magnetoresistance (GMR) in metallic multilayers have been the subjects of intense scientific activity. However, progress in the field has been hampered by inadequate understanding of the underlying mechanisms largely because of the limitations of conventional x-ray scattering and surface imaging methods in resolving the atomic structures of the buried interfaces involved. Here we present definitive cross-section transmission electron microscopy results of permalloy/gold multilayer structures/interfaces and correlate their atomic structure with changes in GMR. In particular, based on quantitative interpretations of high resolution electron micrographs, increased roughening of the interfaces due to the interdiffusion of Au into the permalloy layer and the bridging of the ferromagnetic layers in the multilayer stacks have been correlated directly with reduction of GMR on annealing.

## Applications of Electron Microscopy to Materials Science

Nukleonika 39 1-2 141 1994

Basic methods used in conventional and high resolution electron microscopy are briefly reviewed including the parameters limiting resolution. In addition, advantages of convergent beam electron diffraction are discussed. Two specific examples (the role of stoichiometry in GaAs layers grown by molecular beam epitaxy at low temperature, and defects formed at InGaAs/GaAs heterointerfaces) illustrating applications of electron microscopy to the understanding properties of semiconductor heterolayers are described. Electron microscopy is revealed as a very powerful tool in solving problems in material science. It is extremely useful for achievement of desired optical and electrical characteristics.

---

36902

M

R

S.Q. Xiao, S.A. Maloy, A.H. Heuer and U. Dahmen

## Morphology and Interface Structure of $\text{Mo}_5\text{Si}_3$ Precipitates in $\text{MoSi}_2$

Phil. Mag. A (in press)

Two distinctly different morphologies of  $\text{Mo}_5\text{Si}_3$  precipitates have been observed in a single crystal  $\text{MoSi}_2$ . Both precipitates are laths elongated along the  $\langle 110 \rangle$  direction common to the matrix and the precipitate, but differ in their cross-sectional shape and lattice orientation. Type I precipitates exhibit a rectangular cross section, with interfaces parallel to low-index planes  $(110)_m \parallel (002)_p$  and  $(002)_m \parallel (220)_p$ , while type II precipitates are parallelograms, with their major interface at  $13^\circ$  to the low-index planes  $(002)_m \parallel (220)_p$ , (the subscripts m and p denote the  $\text{MoSi}_2$  matrix and  $\text{Mo}_5\text{Si}_3$  precipitate, respectively). The orientation relationships corresponding to the two characteristic morphologies differ by a  $1.8^\circ$  rotation around the lath axis. A periodic array of dislocation loops and associated ledges enveloping the precipitates were revealed by high resolution electron microscopy and selected area electron diffraction. The Burgers vector of these dislocations was determined unambiguously from high resolution images in orthogonal viewing directions. The differences between the two characteristic morphologies and their orientation relationships are due to a difference in the stacking sequence of ledges.

**Comparison Between Photoluminescence and Raman Scattering in Disordered and Ordered Alloys of GaInP**Phil. Mag. B. 70 3 453 1994

We have studied the photoluminescence spectra in both ordered and disordered phases of  $\text{Ga}_{0.3}\text{In}_{0.5}\text{P}$  alloy as a function of pressure. We found evidence of a pressure-induced conversion of  $\text{Ga}_{0.3}\text{In}_{0.5}\text{P}$  from a direct band gap semiconductor to an indirect band gap semiconductor owing to lowering of the X conduction band valleys relative to the minimum at the zone center. Raman spectra in  $\text{Ga}_{0.3}\text{In}_{0.5}\text{P}$  electronic Raman scattering from single-particle excitations indicates the existence of a high-density electron gas which is absent in a similarly doped disordered sample.

---

35394

M

No

M. Goldman, C.P. Burmester, L.T. Wille and R. Gronsky

**Strain and Domain Evolution in  $\text{YBa}_2\text{Cu}_3\text{O}_x$** Phil. Mag. Letts. 70 65 1994

A Monte Carlo study of the time evolution of atomic positions and occupancies within the basal plane of  $\text{YBa}_2\text{Cu}_3\text{O}_x$  is performed. The simulations are based upon an anisotropic Ising model, and, for the first time, include elastic interactions associated with continuous displacements at atoms within the basal plane. Samples quenched to temperatures below the disorder-order transition curve from the disordered, tetragonal state rapidly form orthorhombic domains separated by twin boundaries. The resulting microstructure is observed to coarsen and eventually anneal into a single domain that exhibits the experimentally observed superlattice reflections. Strain maps are used to elucidate and interpret these observations.

S. Schuppler, S. Friedman, M. Marcus, D. Adler, Y. Xie, F. Ross, T. Harris, W. Brown, Y. Chabal, L. Brus and P. Citrin

### **Dimensions of Luminescent Oxidized and Porous Silicon Structures**

Phy. Rev. Letts. 72 16 2648 1994

X-ray absorption measurements from H-passivated porous Si and from oxidized Si nanocrystals, combined with electron microscopy, ir-absorption,  $\alpha$ -recoil, and luminescence emission data, provide a consistent structural picture of the species responsible for the visible luminescence observed in these samples. The mass-weighted average structures in por-Si are particles, not wires, with dimensions significantly smaller than previously reported or proposed.

---

34582

M

R

M. Goldman, C.P. Burmester, L.T. Wille and R. Gronsky

### **Deformation Superstructures, Tweed, and Oxygen Vacancy Ordering Associated with Phase Transformations in $\text{YBa}_2\text{Cu}_3\text{O}_z$**

Phys. Rev. B. 50 2 1337 1994

A new theoretical technique is described, employing Monte Carlo simulation, which allows the investigation of strain effects associated with transformations in solids. The method applies a grand canonical stress ensemble in the study of elasticity during phase evolution in  $\text{YBa}_2\text{Cu}_3\text{O}_z$ , where both oxygen occupancy and atomic positions in the basal plane, as well as total sample volume, can vary. Quenching experiments yield both metastable square root  $2a_0 \times \text{square root } 2a_0$  superstructures from short wavelength modulations and a "tweed" texture from long period  $\langle 110 \rangle$  modulations of the ordered  $z = 7.0$  compound.

**Epitaxial Growth Mechanisms and Structure of  $\text{CaF}_2/\text{Si}(111)$** Phys. Rev. B 50 19 14 1994

The early stages of interface formation between  $\text{CaF}_2$  and  $\text{Si}(111)$  have been studied, *in-situ*, by a combination of reflection high energy electron diffraction, x-ray diffraction and core-level photoemission. The results are combined with ex-situ transmission electron microscopy to show that the initial growth mode changes from Volmer-Weber to Stranski-Krastanow, depending on the substrate temperature. The crossover is correlated with a submonolayer transition from the  $\text{Si}(111)$ -(7 x 7) to a (3 x 1) reconstruction. This is accompanied by fluorine dissociation at the interface. Both initial growth modes can lead to a uniform  $\text{CaF}_2$  epilayer and subsequent growth on this surface is layer by layer. Using x-ray crystal truncation rod analysis, we have examined the  $\text{CaF}_2/\text{Si}(111)$  surface and interface structure. For films grown at temperatures above the (7 x 7) - (3 x 1) transition, the Ca atom in the  $\text{CaF}$  layer at the interface is located in a single  $T_4$  bonding site. Finally, we have observed a structural transition at the interface from the as-grown structure to a  $\sqrt{3} \times \sqrt{3}$  R 30° reconstruction, which appears to be incommensurate. The dynamics of this transition and the possible mechanisms will be discussed.

36173

M

R

L.T. Romano, R.D. Bringans, J. Knall, D.K. Biegelsen, A. Garcia, J.E. Northrup and M.A. O'Keefe

**Atomic Rearrangement at the Interface of Annealed  $\text{ZnSe}$  Films Grown on Vicinal  $\text{Si}(001)$  Substrates**Phys. Rev. B 50 7 4416 1994

Significant atomic rearrangement at the interface was found to take place after post-growth annealing treatments of epitaxial  $\text{ZnSe}$  on As-passivated  $\text{Si}(001)$  substrates which were tilted by 4° towards the [110] direction. The thermal stability of the  $\text{ZnSe}/\text{As}/\text{Si}$  interface was studied by rapid thermal annealing at temperatures up to 960° C after growing an epitaxial  $\text{GaAs}$  cap layer to prevent evaporation of the  $\text{ZnSe}$  during the anneals. The  $\text{ZnSe}/\text{As}/\text{Si}$  interface was examined by high-resolution electron microscopy. After an anneal at 900° C the  $\text{ZnSe}/\text{As}/\text{Si}$  interface transformed from an atomically smooth interface found in the as-grown films to a faceted structure with [111]-oriented sidewalls that extended preferentially in the [110] direction. The 60° dislocations that were previously observed along this direction combined into closely spaced pairs or into Lomer dislocations which were associated with the facets. We present a model for the atomic structure of the faceted interface which is consistent with the experimental data and satisfies electron-counting considerations. Total-energy calculations of the  $\text{ZnSe}/\text{As}/\text{Si}(001)$  interface were compared with those for the [111] interfaces seen after faceting.

**Observation of Hendricks Teller Partial Order in a Tetragonal Cuprate Superconductor:  $\text{La}_{1.68}\text{Nd}_{0.14}\text{Na}_{0.10}\text{K}_{0.082}\text{CuO}_4$** Phys. Rev. B. 50 13 9419 1994

The cuprate superconductor  $\text{La}_{1.68}\text{Nd}_{0.14}\text{Na}_{0.10}\text{K}_{0.082}\text{CuO}_4$ , was prepared by selective precipitation from a NaOH/KOH eutectic melt at 350°C. Synchrotron x-ray-diffraction data indicate that the structure is related to the tetragonal T-structure type of doped  $\text{La}_2\text{CuO}_4$ , but the presence of superlattice reflections shows the unit cell to be tripled along the c direction [ $a = 3.763(1) \text{ \AA}$  and  $c = 39.63(2) \text{ \AA}$ ]. The existence of this supercell is confirmed by electron microscopy and electron diffraction, which show that the tripling is due to cation ordering. Careful examination of the positions and widths of the superlattice reflections in the synchrotron data indicates that the dopant cations are in fact only partially ordered, and a simple Hendricks-Teller model using an ordering scheme suggested by the electron microscopy data agrees well with the diffraction data. There is no structural change (orthorhombic distortion) between room temperature and 28 K, just above the onset temperature for superconductivity determined from magnetic-susceptibility measurements. The Meissner fraction, estimated to be 80% at 5 K, indicates that this material is a bulk superconductor.

**Sn Submonolayer-Mediated Ge Heteroepitaxy on Si (001)**Phys. Rev. B. (in press) 15 1995

The influence of a Sn submonolayer on the growth mode of Ge on Si (001) during molecular beam epitaxy has been studied by transmission electron microscopy and reflection high-energy electron diffraction. It was found that Sn-mediated growth promotes Ge island formation, suggesting that Sn acts to enhance the surface mobility of Ge adatoms. It is pointed out that being able to uniformly cover and strongly segregate to the growing surface is necessary, but not sufficient, for a surfactant to effectively suppress Ge islanding on Si.

**The Role of Elasticity Associated with Oxygen Ordering in  $\text{YBa}_2\text{Cu}_3\text{O}_x$** 

Phys. Rev. B (submitted)

A Monte Carlo technique incorporating elasticity is applied to simulate oxygen-vacancy ordering and concomitant elastic distortion within the basal plane of  $\text{YBa}_2\text{Cu}_3\text{O}_x$ . Simulations performed with this model are first compared to previous studies of oxygen-vacancy ordering under a static lattice approximation, and then used to investigate the contribution of elastic strain to the formation of experimentally observed  $2\sqrt{2}$  superstructures, deformation twinning, twinning, nucleation and growth of ordered domains, and the nature of the tetragonal-to-orthorhombic transition occurring in this system. The influence of elasticity on microstructural evolution is examined via simulations of rapid quenching through the tetragonal-to-orthorhombic transition or of deformation of the orthorhombic phase to induce strain, both followed by annealing. The formation and evolution of these microstructures are rationalized in terms of the accommodation of strain energy accumulated during the course of the simulated thermo-mechanical treatments.

**TEM Investigation of Multilayered Structures in Heterogeneous Au-Co Alloys**Phys. Stat. Sol. A 147 165 1995

The microstructure of melt-span  $\text{Au}_{83.3}\text{Co}_{16.7}$  and  $\text{Au}_{71.6}\text{Co}_{28.4}$  ribbons is investigated by means of analytical and high-resolution electron microscopy. The as-quenched ribbons contain a multilayered lamellar eutectic within the grains and Co precipitates at grain boundaries. Cobalt-rich lamellae are found with growing direction  $\langle 110 \rangle$  and an average width of 7.5nm. The thickness of the Co-lamella parallel to  $[001]$  is larger in the sample with the higher Co-content. Annealing at 480° C dissolves the eutectic and large Co particles are formed at grain boundaries and within the grains deteriorating the magnetic properties.

**Microscopic Model and Computer Simulation of Detwinning in  $\text{YBa}_2\text{Cu}_3\text{O}_x$** Physica C 230 16 1994

The results of Monte Carlo simulations of the detwinning of the high-temperature superconductor  $\text{YBa}_2\text{Cu}_3\text{O}_x$  are reported. To study the effects of detwinning and the concomitant domain growth in this system, a sample is first produced having a representative domain structure using Monte Carlo simulation at fixed temperature and oxygen chemical potential based on an asymmetric two-dimensional Ising-model. The resulting microstructures typically consist of finely textured orthogonal domains indicative of a twinned structure. Next, a symmetry-breaking detwinning potential is imposed and the time evolution of the system is followed. At low temperatures or detwinning potentials only partial detwinning is typically achieved as the system is often frozen in 'glassy' domain structures, but at higher temperatures or detwinning potentials complete detwinning is attained. Domain kinetics is mapped out as a function of oxygen chemical potential and temperature and evidence is presented for an algebraic domain growth law of the form  $t^n$  with  $n$  between 0.33 and 0.75 depending on the control parameters.

**High Resolution Analyses and Interfacial Design of Inorganic Materials**Scripta Met. et Mat. 31 8 953 1994

High resolution microscopy, diffraction, and microanalyses have been used to study fundamental aspects related to interfaces in a range of inorganic materials including multilayers, ceramics, composites, nanostructures, etc. Although these materials differ widely in nature and composition, the basic problems of characterization are generic. As the scale of structure decreases, the importance of interfaces increases, since the physical properties depend on the surface/volume ratio and morphology of the phases present, and the requirements for structural characterization and synthesis become more stringent. This paper gives a brief review of some examples of such studies which have led to ideas for tailoring microstructures (interface control) and the emphasis on processing needed to achieve such structures.

## On the Research, Development, and Exploitation of Magnetic Materials

Scripta Met. et Mat. 30 6 671 1994

Historically, since the discovery of the unique properties of lodestone, magnetic materials have been technologically important. In comparison with mechanical, semiconducting, and other materials, magnetic materials are not being investigated with nearly sufficient effort, although they are vital for a wide variety of devices, technologies and industries using permanent, soft and hard magnets. Some uses include electric motors, information storage systems and medical instrumentation. Total dollar value for the recording industry alone has been estimated to be \$100 billion worldwide and, in the U.S., several billion dollars for permanent magnets by the year 2000. This paper summarizes recent developments in ordered  $L1_0$  type magnets and multilayer magnetic structures. The thin film multilayers are candidates for new types of magnetoresistive (MRI) heads capable of substantially improving the capacity of hard disk storage systems. The study of materials having the  $L1_0$  structure yields basic insights into structure-property relationships that are applicable to other ordered magnets such as the Fe/Si/Al Sendust alloys considered for recording heads. It is our aim to make a few general comments on magnetic materials research in general and discuss a few specific ongoing projects.

---

35853

A R

N. Thangaraj, K.M. Krishnan, and R.F.C. Farrow

## Microstructural Evolution and Giant Magnetoresistance in Granular and Multilayer Magnetic Thin Films

Scripta Met. et Mat. (accepted)

Evolution of microstructure in both granular  $M_xAg_{1-x}$ , ( $M = \text{Co, Fe}$ ) and multilayer permalloy (Py)/Au magnetic thin films have been studied by electron microscopy and correlated with their magnetoresistive properties. In particular, the atomic structure/interface roughness (multilayers) and the particle size/shape distribution (granular alloys) were observed. For granular alloy thin films, a uniform size distribution of magnetic particles, optimally peaked at  $\sim 20\text{\AA}$  diameter, is suggested for enhanced GMR. As growth Py/Au multilayers exhibit a sharp interface but with growth twins and periodic array of misfit dislocations. Annealing of these multilayers results in an enhanced interface roughness, disappearance of the Au layers, causing a local breakdown of the antiferromagnetic coupling and a deterioration in the observed GMR. Finally, microstructure and GMR of granular films processed by novel ion-implantation routes will also be discussed.

**Dynamic Observations of Interface Motion During the Oxidation of Silicon**Surface Science 310 243 1994

We describe real time observations of the behavior of the silicon-oxide interface during oxidation *in situ* in an ultra high vacuum transmission electron microscope. We have formed clean, flat Si (111) surfaces by heating under UHV and allowed oxidation or oxygen etching to proceed in the microscope. We have examined the kinetics of both the oxidation and etching reactions using an imaging technique based on the use of forbidden reflections in silicon. We find that oxidation to form SiO<sub>2</sub> occurs by the reaction of discrete monolayers with no flow of surface steps. This is in dramatic contrast to oxygen etching, during which the volatile oxide SiO evaporates preferentially from step edges.

---

un-numbered

M

R

X.W. Lin, W.V. Lampert, W. Swider, T.W. Haas, P.H. Holloway, J. Washburn and Z. Liliental-Weber

**Morphology of Al-Ni-Ge Ohmic Contacts to n-GaAs as a Function of Contact Composition**Thin Solid Films 253 490 1994

Al-Ni-Ge ohmic contacts on n-GaAs(001) were prepared by sequential vapor deposition and subsequent annealing at 500° C. Structural properties were studied as a function of contact composition by transmission electron microscopy and scanning electron microscopy, in addition to other techniques. Al was deposited as the top layer at a fixed thickness. While all metalizations exhibit a non-spiking interface with the GaAs substrate, it was found that the contact morphology varies strongly with the Ge:Ni thickness ratio. For a Ge:Ni thickness ratio of 3:4 or greater, annealing results in the formation of a thick Al<sub>3</sub>Ni layer adjacent to the GaAs substrate, as well as a non-uniform surface layer, characterized by dendritic Ge precipitates in an Al matrix. By lowering the Ge:Ni thickness ratio to 1:2, the surface morphology was greatly improved and the contact displays a stable layered structure of the type Al<sub>3</sub>Ni/(Ni-Ge)/GaAs. These result were accounted for on the basis of a recently developed Al-Ni-Ge ternary phase diagram.

## Microstructural Analyses of Advanced Inorganic Materials

Ultramicroscopy 54 145 1994

Modern technology depends critically on advanced materials, e.g., in transportation, communications, data processing, production systems, etc., and more and more emphasis is being placed on research and development of materials. In order to tailor materials to meet specific performance requirements (mechanical/physical properties), it is essential to understand the relationships - synthesis and processing, structure, performance. Processing develops microstructure, mesostructure and chemical distribution of the components. These in turn determine properties. In order to characterize these features, high resolution techniques such as electron microscopy, microdiffraction and microanalysis are required. This paper gives two examples of the applications of electron microscopy to understanding and developing advanced ceramics, viz. silicon nitride and aluminum nitride.

---

36753

M

No

S. Paciornik, R. Kilaas, J. Turner and U. Dahmen

## A Pattern Recognition Technique for the Analysis of Grain Boundary Structure by HREM

Ultramicroscopy (submitted)

A pattern recognition technique for the detection of structural units in high resolution images of interfaces is described. The technique uses cross correlation functions as a means of locating atomic patterns characteristic for an interface and as a measure of similarity between related units. Application is not limited to periodic, or even to planar interfaces. Characteristic structural units can be extracted from an experimental image and some important parameters such as mirror or mirror glide symmetry, and rigid body displacements can be determined without knowledge of the imaging parameters. The technique allows an image of a structural unit with reduced specimen noise to be obtained by averaging over several similar units, even if a boundary is not periodic and not planar. Characteristic structural units so determined can subsequently serve as a basis for structure determination by a refinement process image simulations optimized for several experimental parameters.

un-numbered                      A                      No

X.Y. Song, W. Cao and A.J. Hunt

### **Three Dimensional Shapes of Particles and Pores in Silica Aerogels by HRTEM**

4th Sym. on Aerogels      10. 1994

We have used tilt and rotation techniques on high-resolution transmission electron microscopy (HRTEM) to examine and compare both the particle and pore shapes between the two-dimensional image and the real structures in silica aerogels. The samples studied are made from based-catalyzed TEOS gels; one is pure silica aerogel and the other is aerogel containing iron compounds introduced by the thermal decomposition of ferrocene at about 120° C.

---

35516                                      A                                      No

M.A. O'Keefe and V. Radmilovic

### **Specimen Thickness is Wrong in Simulated HRTEM Images**

Proc. 13th ICEM      1 361 1994

Simulated high-resolution transmission electron microscope (HRTEM) images can accurately reproduce experimental HRTEM images only when imaging parameters are accurately known. The most difficult parameter to measure accurately is the specimen thickness. In matches between experimental and simulated HRTEM images, specimen thickness is often regrettably treated as a disposable parameter; i.e. the experimental specimen thickness is not measured, but assumed to be the thickness at which the simulated image best matches the experimental one. Such a procedure can result in seriously-underestimated specimen thicknesses, since a simulated crystal must always be thicker than an experimental one to produce the same image. Sometimes the matching thickness at the known defocus appears ridiculously small and a greater thickness is selected (incorrectly) by taking advantage of the trade-off between objective defocus and specimen thickness. With increasing specimen thickness, simulated images attain a specific image character faster than do experimental ones because simulated scattering is more dynamical, since simulated specimens are positioned exactly on-axis and experimental specimens are not.

un-numbered                      A                      No  
K.H. Downing, M.A. O'Keefe and H.-R. Wenk

### **Oxygen Contrast in Ionic Structures: 3D Electron Crystallography of YBCO.**

Proc. 13th ICEM    1 475 1994

We report on direct phase determination from high resolution images and reconstruction of the structure of the orthorhombic YBCO ( $\text{YBa}_2\text{Cu}_3\text{O}_{7-\delta}$ ) high temperature superconductor from high resolution images in five different directions. High resolution images were obtained with the JEOL ARM-1000 atomic resolution microscope at 800keV with a spherical aberration of 2mm and a point-to-point resolution of 1.6Å. From negatives near Scherzer focus, enlarged prints were produced. Small areas of the prints were scanned and digitized images were then Fourier transformed. Amplitudes and phases were extracted for all  $hkl$  reflections above a defined signal to noise ratio. Phases were then shifted to a common origin, using reference reflections based on the known crystal structure and symmetry considerations. Data from the five sections were combined and a Fourier synthesis revealed a 3d distribution of the electron potential. Experimental data compare well with a reconstruction based on amplitudes and phases obtained from simulations assuming multibeam scattering. The good agreement between structure and 3d potential map illustrates that it is straightforward to extract information on cation locations from routine electron crystallography on very small sample areas.

---

un-numbered                      A                      No  
Z. Liliental-Weber

### **Evolution of As Precipitates in Annealed Low-Temperature-Grown GaAs Layers**

Proc. 13th ICEM    2A 599 1994

Growth of GaAs layers (LT-GaAs) by molecular beam epitaxy with As overpressure in the temperature range close to 200° C produced very interesting structural and electronic properties for the layers. Incorporation of excess As was observed in the layers which causes expansion of the lattice parameter. The lower the growth temperature the more As was incorporated and the larger the expansion of the lattice parameter. This excess As is in the form of a high density of  $\text{As}_{\text{Ga}}$  antisite defects confirmed by EPR (about  $10^{20} \text{ cm}^{-3}$ ) as well as interstitial As confirmed by PIXE.

un-numbered                      A                      No

N.D. Zakharov, Z. Liliental-Weber, V.P. Filonenko, I.P. Zibrov and M. Sunderberg

## **HREM Studies of Some Neodymium-Doped Tungsten Oxides**

Proc. 13th ICEM    2B 865 1994

High resolution electron microscopy (HREM) has been a very useful tool in the structure investigations of tungsten oxides, prepared at high pressure ( $P = 50$  kbar) in combination with high temperature ( $T = 1773$  K). Recently, the structures of the high-pressure phases,  $WO_{2.625}$  (Barabanenkov et al 1993),  $W_3O_8(I)$  and  $W_3O_8(II)$  (Sundberg et al 1993) were deduced from HREM images. Here we report some HREM results obtained from a Nd-doped tungsten oxide sample ( $WO_3 : Nd_2O_3 = 9:1$ ) synthesized at high pressure ( $P = 50$  kbar,  $T = 1573$  K). The HREM images were taken with the ARM microscope at Lawrence Berkeley Laboratory.

---

37263                      A                      No

L. Normand, R. Kilaas, Y. Montardi and A. Thorel

## **Structure of 90° Domain Walls in Ferroelectric Barium Titanate Ceramics**

Proc. 4th Europ. Cer. Soc.

The study of domain walls in ferroelectric materials is of great industrial and scientific interest because it may reveal their influence on many material characteristics, such as permittivity, and piezoelectric constants, etc. We have studied the atomistic structure of 90° domain walls in pure and doped barium titanate ceramics in its tetragonal ferroelectric phase using high resolution transmission electron microscopy. A computerized method has been developed to map and to measure quantitatively the field of displacements of the experimental lattice in relation to a perfect lattice created from a non-distorted region of the HREM image.

**Defects Formed at the InGaAs/GaAs Interface**

Proc. Control Semicond. Interfaces 81 1994

The results of elastic strain relaxation for a system with low misfit and the possibility of an internal source of misfit dislocation formation will be discussed. As an example, layers of  $\text{In}_x\text{Ga}_{1-x}\text{As}$  grown on GaAs will be shown. Anisotropy of  $\alpha$  and  $\beta$  dislocation introduction was observed for layers grown on an (001) substrate. The anisotropy was drastically enhanced by substrate tilting. Migration of In toward the surface and into the substrate was observed, even for layer thicknesses below the critical layer thickness for misfit dislocation formation. The In segregation also resulted in formation of platelets rich in In near the InGaAs/GaAs interface, and decoration of misfit dislocations by In. The local strain associated with such platelets may be large enough to promote the nucleation of dislocation loops which can be considered as a source of misfit dislocations. It is also found that during post-growth annealing,  $60^\circ$  dislocations along  $\langle 110 \rangle$  directions tend to move by climb toward the  $\langle 100 \rangle$  orientation.

37394

A

No

K.M. Krishnan and A.R. Modak

**Epitaxy and Magnetotransport Properties of  $\text{La}_{1-x}\text{Sr}_x\text{MnO}_3$  ( $x=0.2-0.3$ ) Films Synthesized by Both Pulsed Laser Deposition and Novel Chemical Routes**

Proc. Fall MRS (submitted)

Alkaline earth substituted manganese oxides,  $\text{La}_{1-x}\text{A}_x\text{MnO}_3$  ( $\text{A}=\text{Ca}, \text{Sr}, \text{or Ba}$ ), with perovskite structures, have attracted much recent attention because of their very large magnetoresistance for composition in the range  $0.1 < x < 0.4$ . However, the fundamental mechanism governing their galvanomagnetic properties and magnetization behavior is, as yet, not understood. Our recent results, to be discussed in detail, include (a) comparisons of the microstructures of oxide films achieved by PLD and sol-gel routes, (b) studies of epitaxy/polycrystallinity of films grown on different substrates by both methods using x-ray and HRTEM imaging, (c) correlations between microstructure and magnetization/galvanomagnetic properties, and (d) integration with Si.

un-numbered                      M                      No  
L. Normand, R. Kilaas, Y. Montardi and A. Thorel

**Special Crystalline Defects: Ferroelectric Domain Walls in BaTiO<sub>3</sub>**

Proc. GFC  
Paper written in French.

---

35725                      M                      No  
V. Radmilovic and G. Thomas

**Nonstoichiometry of Al-Zr Intermetallic Phases**

Proc. ICAA'94    II 153 1994

Nonstoichiometry of metastable cubic  $\beta'$  and equilibrium tetragonal  $\beta$  Al-Zr intermetallic phases of the nominal composition Al<sub>3</sub>Zr in Al-rich alloys has been extensively studied. It is proposed that the "dark-contrast" of  $\beta'$  core in  $\beta'/\delta'$  complex precipitates, in Al-Li-Zr based alloys is caused by incorporation of Al and Li atoms into the  $\beta'$  phase on Zr sublattice sites, forming nonstoichiometric Al-Zr intermetallic phases, rather than by Li partitioning only.  $\beta'$  particles contain very small amounts of Zr, approximately 5 at.%, much less than the stoichiometric 25 at.% in the Al<sub>3</sub>Zr metastable phase. These particles are, according to simulation of high resolution images, of the Al<sub>3</sub>(Al<sub>0.4</sub>Li<sub>0.4</sub>Zr<sub>0.2</sub>) type. Nonstoichiometric particles of average composition Al<sub>4</sub>Zr and Al<sub>6</sub>Zr are observed in the binary Al-Zr alloy, even after annealing for several hours at 600° C.

**Structural Properties of Multilayered Thin Films**

Proc. ICEM 231 1994

Modern technology relies more and more on advanced materials, and increasing emphasis is being placed on research and development of multilayered thin films. The basic idea behind these superlattices is to combine individual physical properties of the superlattice components in order to tailor superior overall thin film properties for specific applications. The efficiency by which individual properties of superlattice components will generate enhanced thin film properties depends on microstructural conditions which are related to the general structure of superlattices as a stacking of alternating layers of different elements or compounds. Structural properties of interest include epitaxial orientations, layer thickness, internal strains, interfacial roughness and interdiffusion. The objective of this paper is to address the significance of the influence these structural properties have on the physical properties of multilayered thin films using three different examples.

---

36543

A

No

S.Q. Xiao, U. Dahmen, S.A. Maloy and A.H. Heuer

**HREM Characterization of Invariant Line Interfaces and Structural Ledges in Mo-Si Alloys**

Proc. iib95 (submitted)

Two distinctly different morphologies of  $\text{Mo}_3\text{Si}_3$  precipitates have been observed in a  $\text{MoSi}_2$  single crystal matrix. The difference between these two morphologies is analyzed in detail by high resolution electron microscopy and explained by both the invariant line and the structural ledge theory, which are shown to predict identical interfaces.

### **Quantitative Study of the Atomistic Structure of Ferroelectric Domain Walls in Barium Titanate**

Proc. iib95 (submitted)

Barium titanate is a favorable material for theoretical study of ferroelectricity; small amounts of dopants can change drastically its properties, its crystallographic structure is relatively simple and reasonably stable under the beam in the Transmission Electron Microscope. Therefore, a thorough TEM study of various doped barium titanates may lead to fundamental insights of the elementary mechanisms of the ferroelectricity.

---

37369

A

No

A.R. Modak and K.M. Krishnan

### **La<sub>1-x</sub>Sr<sub>x</sub>MnO<sub>3</sub> Thin Films Synthesized by a Novel Polymeric SOL-GEL Process: Structure and Magnetic Properties**

Proc. Magnetism & Mag. Mats.

Thin films of LaMnO<sub>3</sub> doped with Ca, Sr or Ba have recently come into prominence due to reports of their unusually high magnetoresistance (termed colossal magnetoresistance {CMR}). There is an upsurge of research activity addressing questions of both fundamental (with respect to re-examining the physics behind the magnetic/magnetotransport behavior) and technological (with a view of using this material in the next generation magnetoresistive read heads and sensors) importance. We present here a versatile chemical processing route for fabrication of La<sub>1-x</sub>Sr<sub>x</sub>MnO<sub>3</sub> thin films which can be extended to Ca and Ba doped compositions. Key features of this process are its overall simplicity and low cost, compatibility with IC planar technology, low processing temperatures, ease of composition variation, and ability to deposit novel structures such as compositionally graded thin films, multilayers, porous structures, etc. Microstructure and microchemistry of both polycrystalline and epitaxial thin films in relation to the polymer chemistry underlying the process and their magnetic/magnetotransport properties will be discussed.

K.M. Krishnan, A.R. Modak, C.A. Lucas, H.B. Cherry, and R. Michel

### **Role of Epitaxy and Polycrystallinity in the Magnetoresistance and Magnetization of $\text{La}_{0.8}\text{Sr}_{0.2}\text{MnO}_3$ Thin Films**

Proc. Magnetism & Mag. Mats.

Alkaline earth substituted manganese oxides,  $\text{La}_{1-x}\text{A}_x\text{MnO}_3$  ( $\text{A} = \text{Ca}, \text{Sr}, \text{or Ba}$ ), with perovskite structures, have attracted much recent attention because of their very large magnetoresistance for composition in the range  $0.1 < x < 0.4$ . However, the fundamental mechanism governing their galvanomagnetic properties and magnetization behavior, is, as yet, not understood. Moreover, these properties are observed to be dependent on conditions of growth and annealing, composition, oxidation state, epitaxy and the overall microstructure. More detailed characterization of the structure and properties of these films and the epitaxial growth of similar films with well defined grain boundaries is in progress.

T.D. Nguyen, K.M. Krishnan, L.H. Lewis, Y. Zhu and D.O. Welch

### **Electron Microscopy Studies of the Microstructure and Composition in NdFeB-Based Hard Magnet Alloys**

Proc. Magnetism & Mag. Mats.

A detailed comprehension of the microstructure and composition in NdFeB hard magnet alloys is important in understanding their magnetic properties and reversal mechanisms. In this study, transmission electron microscopy (TEM) studies of the grain boundary phases in melt-quenched, thermomechanically-processed magnet alloys based on the  $\text{Nd}_2\text{Fe}_{14}\text{B}$  composition, utilizing high resolution, analytical, and Lorentz techniques, are presented. The relationship between the observed microstructure and magnetic properties, and in particular the reversal mechanism in these materials are discussed.

**Epitaxial  $\text{Fe}_{16}\text{N}_2$  Films Grown on Si(100) by reactive Sputtering**

Proc. MMM

The claim of a giant magnetic moment in  $\alpha'$ - $\text{Fe}_{16}\text{N}_2$  is still under considerable scrutiny. The controversy is fueled by the widely varying magnetization values observed by different workers, and by the lack of reproducibility of the pure phase and giant moment under practical constraints. Pure  $\alpha'$  films with a giant moment of 2.9 T have only been grown on the complex substrate,  $\text{In}_{0.2}\text{Ga}_{0.8}\text{As}$ , and attempts at growth on simpler substrates have resulted in only a modest enhancement in moment and often in multiphase mixtures. We have successfully grown pure epitaxial  $\alpha'$ - $\text{Fe}_8\text{N}$  (N martensite) and  $\alpha'/\alpha''$  films, as well as pure  $\gamma$  and pure  $\alpha$  films, and measured the magnetic properties of each phase. Preliminary vibrating sample magnetometry data on  $\alpha'$  indicate an enhanced magnetic moment with respect to pure Fe. Results from transmission electron microscopy, electron energy loss spectroscopy, and conversion electron Mössbauer spectroscopy will be presented to elucidate the nature of Fe-N bonding and N ordering as they relate to magnetic properties in  $\alpha'$  and  $\alpha''$ .

---

33478

M

P

F.M. Ross, R. Hull, D. Bahnck, J.C. Bean, L.J. Peticolas, R.R. Kola and C.A. King

**Changes in Electronic Device Properties During the Formation of Dislocations**Proc. MRS 280 483 1994

We describe the results of an investigation into the formation and properties of dislocations in electronic devices. We have made electron transparent specimens from metastable GeSi/Si p-n junction diodes and introduced dislocations into the devices by heating *in situ* in the electron microscope. A modification made on the specimen holder for our microscope enables us to measure the characteristics of these devices while they remain under observation in the microscope. We can therefore observe the changes in the electrical properties of the devices as dislocations form. We confirm that the introduction of dislocations has a deleterious effect on parameters such as the reverse leakage current through a diode. However, the magnitude of the effect we observe cannot be explained by a generation-recombination process and instead, we suggest a model based on the creation of point defects or the diffusion of metals during the formation of dislocations. We also consider the kinetics of dislocation formation, and in particular how the extent of dislocation formation in a device depends on the subsequent processing steps which it undergoes.

unnumbered                      M                      No

R.F. Marks, R.F.C. Farrow, G.R. Harp, S.S.P. Parkin, T.A. Rabedeau, M.F. Toney, A. Ceboliada, N. Thangaraj, et al.

### **Giant Magnetoresistance and Structure of Phase Segregated Metals**

Proc. MRS    313 411 1994

Giant magnetoresistance, GMR, in thin metal films elicits attention due to its technological potential as well as its relevance to theory of exchange coupling. Epitaxial, phase-segregated ferromagnet/paramagnet mixtures have been grown by UHV evaporation. Such films show spontaneous formation of ferromagnetic clusters, and large values of GMR (40% at room temperature) as grown. The growth of Co-Cu, Co-Ag, Fe-Ag, and permalloy-Ag films are described. Structural analysis by grazing-incidence small angle x-ray scattering (GISAXS) provides a measure of cluster size and characteristic spacing. Effects of growth temperatures and subsequent annealing on GMR and film structure are described. Preliminary results of TEM examination of (001) Fe-Ag and Co-Ag granular films are presented for the first time.

---

un-numbered                      M                      No

S. Im., J. Washburn, R. Gronsky, N.W. Cheung, K.M. Yu and J.W. Ager

### **Reducing Dislocation Density by Sequential Implantation of Ge and C in Si**

Proc. MRS    298 139 1994

Carbon implantation was performed after high dose Ge implantation into [100] oriented Si substrates to study the effect of sequential implantation on dislocation nucleation. When the nominal peak concentration of implanted C is over 0.55 at%, dislocations in the SiGe layer containing C are considerably reduced in density after solid phase epitaxial (SPE) annealing at 800° C for 1 hour, compared to the SiGe layer without C. These results suggest that during annealing, C atoms compensate the Ge-induced misfit strain which causes dislocation generation in the region of peak Ge concentration. Channeling spectra obtained by RBS analysis show only 5% to 6% minimum back scattering yield as C atoms suppress the dislocation generation.

### Stress Relaxation in Sputtered W Films and W/GeSi/Si Heterostructures

Proc. MRS 318 697 1994

We have investigated the relationship between microstructures and stress in very thin sputtered W films. We discuss features of the microstructure, in particular the presence of voids in compressively stressed films, in terms of the evolution of the structure from a metastable  $\beta$ -phase. By developing a novel specimen geometry for the transmission electron microscope (TEM), we present dynamic observations of the  $\beta$ -W  $\rightarrow$   $\alpha$ -W transformation.

### Thermal Stability of Epitaxial Al/Si Interfaces

Proc. MRS IX 247 1994

The morphological stability of epitaxial Al/Si interfaces during interdiffusion has been studied by electron microscopy. It was found that Si dissolution in the Al film during annealing and Si precipitation during cooling were both heterogeneous processes, forming Al spikes in the Si substrate and Si precipitates on the Al film, respectively. Dynamic observations during *in-situ* annealing of cross section samples in an electron microscope revealed that spikes nucleated at the junction of Al grain boundaries (gb's) with the Si substrate. Some special grain boundaries did not nucleate spikes. Ex-situ heat treatments showed that the extent and the shapes of spiked regions depended on the interfacial crystallography. From scanning (SEM) and cross-sectional transmission electron microscopy (XTEM) studies, it was found that the Al spikes on Si(100) substrates were hemispherical whereas spikes on Si(111) substrates were disc-shaped.

### 3 D Imaging of Crystals at Atomic Resolution

Proc. MRS 332 563 1994

Electron crystallography has now been used to investigate the structures of inorganic materials in three dimensions. As a test of the method, amplitudes and phases of structure factors were obtained experimentally from high resolution images of staurolite taken in a number of different projections. From images in five orientations, a three-dimensional Coulomb potential map was constructed with a resolution of better than 1.4Å. The map clearly resolves all the cations (Al,Si,Fe) in the structure, and all of the oxygen atoms. This method promises great potential for structure determinations of small domains in heterogeneous crystals which are inaccessible to x-ray analysis. Three-dimensional structure determinations should be possible on small domains only approximately 10 unit cells wide, and may resolve site occupancies in addition to atom positions. Given a microscope stage with a suitable range of tilt and enough mechanical stability, the method could also be applied to small crystalline particles larger than about 50Å to 100Å. In addition, with sufficient computing power, it may be possible to apply the method to derive the two-dimensional structure of periodic defects.

---

35626

M

No

X.Y. Song, W. Cao and A.J. Hunt

### AEM and HREM Evaluation of Carbon Nanostructures in Silica Aerogels

Proc. MRS 349 269 1994

Nanostructured carbon has been deposited in silica aerogels by chemical vapor infiltration using acetylene or ferrocene at moderate temperatures. Using analytical electron microscopy and high-resolution electron microscopy, we have observed various carbon rings and nanotubes in the silica aerogel-based carbon composite. Both X-ray microanalysis and nano-probe diffraction techniques have been used to confirm the presence of those carbon nanostructures. The morphologies and structural properties of the carbon nanotubes and rings have also been examined in detail.

un-numbered                      M                      No  
Z. Weng-Sieh, T.D. Nguyen and R. Gronsky

### **Stability of Ruthenium Silica Bilayer Structures**

Proc. MRS    343 149 1994

The microstructural evolution of ruthenium-silicon dioxide bilayer structures upon annealing is studied using transmission electron microscopy.  $\text{SiO}_2/\text{Ru}/\text{SiO}_2$  structures, with thicknesses of 2/1/2 nm, 4/2/4 nm, 8/4/8 nm, and 20/10/20 nm, are formed by magnetron sputtering and annealed at 300 or 600° C. As-deposited films have grain sizes on the order of the Ru film thickness. After annealing at 600° C, significant grain growth is observed for all thicknesses, such that the final grain sizes are approximately 3 to 20x greater than the original film thickness. The largest increase in the average Ru grain size is observed for the 2 nm thick ruthenium film possibly due to the coalescence of Ru grains. The coalescence of the Ru particles in the 1 and 2 nm thick films results in the formation of lamellar Ru grains, which disrupts the contiguity of the Ru film. In all other cases, the increase in grain size is attributed to normal grain growth, but the formation of anomalous spherical grains is also observed.

---

35286                      M                      No  
Z. Liliental-Weber, H. Fujioka, H. Sohn and E.R. Weber

### **Improvement of the Structural Quality of GaAs Layers Grown on Si with LT-GaAs Intermediate Layer**

Proc. MRS    325 377 1994

Superior electrical and optical quality of GaAs grown on Si with an inserted low-temperature (LT)-GaAs buffer-layer was demonstrated. Photoluminescence intensity was increasing and leakage current of Schottky diodes build on such a structure was decreasing by few orders of magnitude. These observations were correlated with structural studies employing classical and high-resolution transmission electron microscopy (TEM). Bending of the threading dislocations and their interaction was observed at the interface between a cap GaAs layer and the LT-GaAs layer. This dislocation interaction results in the reduction of dislocation density by at least one order of magnitude or more compared for the GaAs layers with the same thickness grown on Si. The surface morphology of the cap GaAs layer is improving as well.

### **Correlation Between the Microstructures and the Electrical Properties of Ni/Au/Te/Au Contacts on n-GaAs**

Proc. MRS 337 295 1994

The structural evolution of Ni/Au/Te/Au contacts on n-GaAs (001) was examined in correlation with their electrical properties as a function of rapid thermal annealing in the temperature range 350-600° C. It was found that heating at temperatures  $\geq 550^\circ$  C results in the formation of ohmic contacts, while contacts annealed at lower temperatures remain nonohmic. Transmission electron microscopy revealed that heating  $\geq 450^\circ$  C leads to extensive reactions between Ni/Au/Te/Au and GaAs and deep spike formation into the GaAs. The major reaction products were identified as NiAs and  $\beta$ -AuGa.  $\text{Ga}_2\text{Te}_3$  grains, growing epitaxially on GaAs, were detected only in the 550° C annealed samples. Heating to 600° C caused considerable  $\text{Ga}_2\text{Te}_3$  loss. Implications of these results concerning the ohmic contact formation mechanism are discussed.

---

35855

A

No

V. Radmilovic and M.A. O'Keefe

### **Effect of C-C Bond Relaxation on the High-Resolution TEM Image of the $\beta$ -SiC Twin Interface**

Proc. MRS (in press)

The effect of bond relaxation on HRTEM imaging of the  $\Sigma 3$  (111) twin interface of  $\beta$ -SiC has been studied by means of high resolution electron microscopy and computer simulation. For comparison with experimental images, series of simulated images were computed for models of the interface in which the distance between carbon atoms ranged from 0.154 nm (typical for an unstrained carbon-carbon bond) to 0.235 nm (a value that has been suggested for the carbon-carbon bond length in  $\beta$ -SiC antiphase boundaries). It was found that the intensity of the spots at the interface in simulated images is very sensitive to the distance between carbon atoms. The best match between experimental and calculated images is obtained with a carbon-carbon atom distance in the neighborhood of 0.188 nm, indicating a significant increase in bond length compared with the unstrained carbon-carbon bond value of 0.154 nm. Measurements of the positions of silicon planes lying next to the interface indicates that the relaxation is not limited to the carbon-carbon bond only, but it is also extended to neighboring silicon-carbon bonds. It appears that image simulations cannot use rigid displacement models for accurate structure determination of the  $\beta$ -SiC twin interface.

---

### **Size, Shape and Crystallinity of Luminescent Structures in Oxidized Si Nanoclusters and H-Passivated Porous Si**

Proc. MRS (in press) 358 1995

Near edge and extended x-ray absorption fine structure measurements from a wide variety of H-passivated porous Si samples and oxidized Si nanocrystals, combined with electron microscopy, ir-absorption,  $\alpha$ -recoil, and luminescence emission data, provide a consistent structural picture of the species responsible for the luminescence observed in these systems. For luminescent porous Si samples peaking in the visible region, i.e.,  $<700\text{nm}$ , their mass-weighted-average structures are determined here to be particles - not wires, whose short-range character is crystalline - not amorphous, and whose dimensions - typically  $<15\text{ \AA}$  - are significantly smaller than previously reported or proposed. These results depend only on sample luminescence behavior, not on sample preparation details, and thus have general implications in describing the mechanism responsible for visible luminescence in porous silicon. New results are also presented which demonstrate that the observed luminescence is unrelated to either the photo-oxidized Si species in porous Si or the interfacial suboxide species in the Si nanocrystals.

### **X-Ray Absorption Spectroscopy from H-Passivated Porous Si and Oxidized Si Nanocrystals**

Proc. MRS (in press) 375 1995

Quantum confinement in nanoscale Si structures is widely believed to be responsible for the visible luminescence observed from anodically etched porous silicon (por-Si), but little is known about the actual size or shape of these structures. EXAFS data from a wide variety of por-Si samples show significantly reduced average Si coordination numbers due to the sizeable contribution of surface-coordinated H. (The H/Si ratios, as large as 1.2, were independently confirmed by ir-absorption and  $\alpha$ -recoil measurements). The Si coordinations imply very large surface/volume ratios, enabling the average Si structures to be identified as crystalline particles (not wires) whose dimensions are typically  $<15\text{ \AA}$ . Comparison of the Size-dependent peak luminescence energies with those of oxidized Si nanocrystals, whose shapes are known, shows remarkable agreement. Furthermore, NEXAFS measurements of the nanocrystals shows the outer oxide and interfacial suboxide layers to be constant over a wide range of nanocrystal sizes. The combination of these results effectively rules out surface species as being responsible for the observed visible luminescence in por-Si, and strongly supports quantum confinement as the dominant mechanism occurring in Si particles which are substantially smaller than previously reported or proposed.

### **Simulation of Multicomponent Thin Film Deposition and Growth**

Proc. MRS (in press)

Results from a multicomponent Monte Carlo simulation of the deposition and growth of  $\text{YBa}_2\text{Cu}_3\text{O}_7$  are presented and discussed. In particular, a detailed examination of the growth modes active during different morphological growth conditions is performed. At higher deposition rates, both [001] and [100] epitaxial variants ('c' and 'a' type growth, respectively) are observed to grow by modes attributed to the classic Volmer-Weber mechanism. At very low deposition rates, the film is observed to grow in a distinct, cyclic, multi-stage process. Small islands of [001] epitaxy nucleate and grow to one unit cell height followed by primarily horizontal growth or "ledge extension" until one unit cell layer has formed. This process then repeats. Simulated RHEED amplitude data from this growth process compares favorably to experimentally obtained data.

### **Microstructures of Amorphous Diamond™ Films Grown by Laser Ablation Method**

Proc. MRS (submitted)

Amorphous Diamond™ (AD) films deposited by laser ablation method show interesting mechanical and electronic properties. In particular, the efficient electron emission from AD films makes them attractive for flat panel display applications. However, the mechanism underlying the associated low work function is still not yet understood; resulting in poor control over material properties. In this work, microstructures of AD films synthesized by laser ablation were characterized using high resolution transmission electron microscopy (TEM), conventional TEM imaging and diffraction, using either parallel illumination or a focused probe of 20nm diameter. Details of these microstructures and their implications on the validity of different electron emission models for Amorphous Diamond™ films will be discussed.

35340

A

No

S.-Q. Xiao, S. Hinderberger, K.H. Westmacott and U. Dahmen

### **Twin Induced Kinetic Shapes of Ge Precipitates in Al**

Proc. MSA 52 692 1994

Twinning plays an important role in the growth of Ge precipitates from solid solution in dilute Al-Ge Alloys. Previous work found a great variety of precipitate shapes and corresponding orientation relationships. At thermodynamic equilibrium only one of these has the lowest free energy, and is therefore the most stable shape. The symmetry of the equilibrium shape must conform to the bicrystal symmetry, i.e. the symmetry of precipitate and matrix superimposed by their orientation relationship. For a twinned precipitate the equilibrium shape is determined by the tricrystal symmetry, i.e. the intersection group of the symmetry of matrix, the precipitate and its twin. This shape is different from that of an untwinned precipitate. For the same reason, twinning can also change the precipitate-matrix interface structure, resulting in preferential growth along certain crystallographic directions. The effect induces non-equilibrium, growth or kinetic shapes. In this report a formation mechanism for the kinetic shapes of Ge precipitates due to twinning is proposed and preliminary TEM observations of the relationship between internal twinning and precipitate shape are presented.

---

35341

A

No

U. Dahmen, N. Thangaraj and R. Kilaas

### **Quantitative TEM Analysis of Microstructural Anisotropy**

Proc. MSA 52 682 1994

Preferred orientation of grain boundaries of interfaces in solids is an important indicator of anisotropy in boundary energy or kinetics. The present study is part of an ongoing investigation of faceting in thin films with the mazed bicrystal microstructure which possesses several unique features that are difficult to measure with standard parameters such as grain size distribution. One of the important characteristics of this microstructure is the degree and type of anisotropy.

**Amorphization of  $\text{Al}_{10}(\text{V}_x\text{Cr}_{1-x})$  Intermetallic Phase**

Proc. MSA 52 662 1994

The stability of phases in alloy systems, including stability in irradiation environments, is *conditio sine qua non* of their engineering applications. Thus, investigations of different phenomena such as compositional variation, segregation, order/disorder transitions and amorphization in different phases under irradiation is of great importance.

**Interpretation of HRTEM Images by Image Simulation: An Introduction to Theory and Practice**

Proc. MSA 52 394 1994

High resolution transmission electron microscope (HRTEM) image simulation was conceived in 1970 in response to a referee's questioning of the interpretation of images of a niobium oxide. Two years later a suite of HRTEM image simulation programs had been established and shown to accurately reproduce experimental HRTEM images when imaging parameters were accurately known. These first simulated images proved that the original interpretation of the niobium oxide images was indeed correct. Once these programs were available, it was possible to explore HRTEM imaging parameters including specimen convergence. Over the twenty years since then, the range of uses of HRTEM simulation has continued to expand, as has the number of programs available.

35349

A

No

L. Normand, A. Thorel and Y. Montardi

**HREM Study of Ferroelectric Domain Wall in Barium Titanate**

Proc. MSA 52 566 1994

This study focuses on high resolution transmission electron microscopy of barium titanate in its tetragonal ferroelectric phase, and especially on the structure of domain walls. This phase is stable between about 0° C and 130° C. During cooling, at 130° C barium titanate changes from a cubic parraelectric phase to a tetragonal ferroelectric phase. In this phase the spontaneous polarization is along one of the six [001] pseudo-cubic directions. Two types of domains can be formed during the phase transition: 90° and 180° domains. In 90° domains the polarization is at 90° from the polarization of the next domain (exactly  $2 \cdot \text{ArcTan}(a/c)$  if  $a$  and  $c$  are the lattice parameters). For these domains the domain walls are  $\langle 110 \rangle$  type planes. In 180° domains the polarization is at 180° from the one in the next domain. 180° domain walls are  $\langle 100 \rangle$  type plane and are assumed to be purely ferroelectric.

35350

A

No

L. Normand, A. Thorel and Y. Montardi

**Fantome: A Calculation of the Dielectric Functions From the Plasmon Excitation**

Proc. MSA 52 990 1994

Electron Energy Loss Spectroscopy is now a well known method for chemical analysis (light elements especially), qualitative analysis of trace elements, EXELFS, etc. The low energy part of the spectrum can also be used in order to perform thickness evaluation and dielectric function determination. When EELS coupled with Transmission Electron Microscopy it presents the great interest of performing all measurements with a spatial resolution of the magnitude of the beam size. In the case of the dielectric function, we can then avoid any average effects due to macroscopic measurements. We then have access to the role of defaults; chemical heterogeneities, grain boundaries, anisotropy which can introduce major modifications in the macroscopic properties. The dielectric measurements are based on Kramers-Kronig analysis of the plasmon excitation: a program ("Fantome") has been written to process the EELS spectra. Results have been obtained on barium titanate.

35351                      A                      R  
V. Radmilovic, H. Gasteiger and P. Ross

### **Structure and Chemical Composition of Pt-Ru Nanoparticle Supported on Carbon Black**

Proc. MSA 52    782 1994

The presence of nanoparticles in catalyst systems is essential because their large surface area increases the reaction rate of the catalyst. However, such a small size of the particles causes serious limitations in microstructural characterization, that could be overcome by high resolution electron microscopy (HREM), especially for particle morphology studies, presence of faults, etc. The present study uses HREM, microdiffraction and EDS techniques to characterize the Pt-Ru catalyst supported on amorphous carbon black. In order to get structural information from local region of single particle, optical diffraction has also been performed. HREM imaging allows the particle morphology and the presence of various structural defects to be revealed. To avoid contamination, microchemical analysis has been performed at -160° C, using cold stage beryllium holder. The fluorescence effect can be neglected.

---

35361                      A                      No  
S. Hinderberger, S.Q. Xiao, K.H. Westmacott and U. Dahmen

### **Shape Training of Ge Precipitates in an Al-1.8 at% Ge Alloy**

Proc. MSA 52    690 1994

Ge precipitates in Al are known to form in a rich variety of shapes and orientation relationships. In this work it is shown that initial non-equilibrium shapes such as plates, laths, needles and tetrahedra can be induced to change to the equilibrium shape of an octahedron by proper temperature cycling. Analysis of this effect in bulk samples was complemented by direct observations of its mechanism during *in-situ* temperature cycling.

### **HREM Analysis of a $\Sigma 5$ (210) Grain Boundary in Rutile**

Proc. MSA 52 726 1994

The present investigation combines HREM with image processing and simulation to determine both the atomic and the step structure of a near  $\Sigma$ -5 (210) symmetrical grain boundary in  $\text{TiO}_2$  (rutile), produce by melt growth from an oriented bicrystal seed. The results of this work leads to the surprising conclusion that there is a local non-stoichiometry at the interface with excess Ti ions, stabilized by a change to a +3 valence state. It is possible that an interfacial non-stoichiometry developed during the process of bicrystal preparation. This conclusion is further supported by the non-stoichiometry observed for the naturally occurring crystallographic shear faults in rutile.

### **Pattern Recognition in HREM Analysis of Grain Boundary Structures**

Proc. MSA 52 934 1994

The present study focuses on an application of pattern recognition techniques to the detection of structural units in grain boundaries and in heterophase interfaces. It describes a simple means of extracting the essential characteristics of an interface from a high resolution image, to find the location, repeat distance and degree of similarity between such units and to sum them into an average unit with increased signal to noise ratio. A measurement of the discrimination between different crystallographic structures can also be obtained from a histogram of the processed image.

**HREM Study of NiO Electrochromic Film and Interface with ITO Layer**

Proc. MSA 52 752 1994

Electrochromic nickel oxide films are of interest in the development of electrochromic devices "smart windows" for a variety of applications including architectural and automotive glazings. Structural characterization of NiO films has been performed by Lampert and Agrawal et al using transmission electron microscopy (TEM), although only in plan view of NiO films which had been deposited on carbon-coated copper grids. However, finer structural features in the NiO electrochromic film and the interface between the NiO film and the indium tin oxide (ITO) layer have not been reported. The purpose of this investigation is to characterize nanometer scale structures in NiO films and the NiO/ITO interface using cross-sectional high resolution electron microscopy (HREM).

---

un-numbered

A

No

W.E. King, M.A. O'Keefe and G.H. Campbell

**Quantitative HREM Using Non-Linear Least Squares Method**

Proc. MSA 52 716 1994

Non-linear least-squares methods have been coupled with high resolution image simulation to determine the critical electron microscopic imaging parameters, such as thickness and defocus, from an experimental image. The method has been extended to include the optimization of atomic column positions and occupancy to determine atomic structure. As an example, the method has been applied to the refinement of the atomic structure of a  $\Sigma 5(310)/[001]$  grain boundary in Nb.

### **HREM Structure Analysis of $\Sigma 13$ Symmetrical Boundaries in Strontium Titanate Bicrystals**

Proc. MSA 53 (submitted)

We have made detailed HREM observations of two  $\Sigma 13$  [001] tilt boundaries in strontium titanate, grown in the (320) and (510) symmetrical orientations, respectively. A rigid body translation has been found only for the (320) boundary which was shown to exhibit mirror glide symmetry. Both interfaces contained steps and pattern shifts consistent with the presence of DSC lattice dislocations. Cross correlation with a structural unit pattern template was applied as a useful technique to analyze the degree of similarity and precise location of characteristic motifs with the HREM images.

### **High Resolution and Diffraction Contrast Imaging of Linear Islands Formed During Molecular Beam Epitaxy**

Proc. MSA 53 (submitted)

There is currently a great deal of interest in the growth and properties of 'one-dimensional' structures. This is motivated by scientific curiosity and by the practical urge to fabricate faster, smaller and more efficient electronic and optical devices. It has recently been reported that under certain conditions linear islands can form spontaneously during growth. In this work we investigate linear  $\text{CaF}_2$  islands which form on Si during molecular beam epitaxy. By combining low resolution diffraction contrast images from plan-view specimens with high resolution images from cross-section specimens, we determine that these islands are extremely uniform in width, can be as narrow as 5 nm, and extend over many 10s of  $\mu\text{m}$ . We postulate a mechanism for the formation of these novel features based on surface energy minimization.

**In Situ Microscopy of the Anodic Etching of Silicon**

Proc. MSA 53 (submitted)

Porous semiconductors represent a relatively new class of materials formed by the selective etching of a single or polycrystalline substrate. Although porous silicon has received considerable attention due to its novel optical properties, porous layers can be formed in other semiconductors such as GaAs and GaP. We are attempting to gain a better understanding of the formation mechanism of porous silicon by allowing pore formation to occur in real time within the electron microscope. We have designed and constructed a specimen holder for a JEOL 200CX featuring a sealed reservoir which can be filled with an electrolyte such as HF. We have carried out ex situ experiments in which the application of 2-3V results in a total current of the order of 0.01 mA and pore growth at 10-100 nm s<sup>-1</sup>.

---

36959 A R

V. Radmilovic and M.A. O'Keefe

**Fresnel Effect in High Resolution TEM Imaging of Small Particles**

Proc. MSA 53 (submitted)

It is established that analysis of Fresnel contrast visible at the edges of nanoparticles in the high resolution electron microscope provides a valuable tool for determining the size of the particles with near-atomic-spacing accuracy. We have used HRTEM image simulation to explore the changes in images of a nanoparticle under various imaging conditions, in particular to relate the model particle size and its apparent size as derived from the HRTEM image. The minimal difference between particle and apparent sizes is obtained at a defocus approximately 400Å below the Gaussian image plane, i.e. close to the Scherzer value for the JEOL ARM 1000 of  $\sqrt{(C_s\lambda)} = 448\text{\AA}$ . At nearly all defocus settings above and below the Scherzer defocus, the spot intensity distribution does not correspond to the positions of the atoms in the particle, especially near a thick edge, leading to an apparent "relaxation" of atom positions near the particle edge. We believe that this effect is due to a strong Fresnel influence on the image, since the deviations between atoms and dots are more pronounced in regions close to the thick edges of small particles, i.e. in regions where the potential drop is sharper. For particles with both thick and tapering edges, this non-uniform "relaxation" may even change the aspect ratio of the particle so that it appears "taller".

---

### **Automated Measurement of Size and Visibility of Small Inclusions in HREM Images**

Proc. MSA 53 (submitted)

This work describes an automatic image analysis method for measuring the visibility and apparent size of inclusions in a matrix, imaged by HREM. The method is based on intensity changes between the matrix and inclusion regions of the image. It provides a quantitative way of describing changes that are generally interpreted only in a qualitative sense. It also allows for measurements in situations of very low visibility where visual estimates are nearly impossible. The method measures the mean squared intensity difference between lines of an image defined as:  $R = \text{mean}[I_m(\mathbf{x}) - I_m(\mathbf{x}_0)]^2$ .  $I_m(\mathbf{x})$  is a line, selected by the user, which is scanned across the image.  $I_m(\mathbf{x}_0)$  is the first line of the scan, taken in a region away from the inclusion. For each position of  $I_m(\mathbf{x})$ ,  $I_m(\mathbf{x}_0)$  is subtracted pixel by pixel, and the average of all squared intensity differences, is obtained ( $R$ ).

### **Modeling and Simulation of Octahedral Pb Inclusions in Al**

Proc. MSA 53 (submitted)

This work describes the modeling and image simulation of octahedral Pb inclusions in Al. A variety of supercells was built, containing Pb inclusions of 2,3,4 and 5 moiré spacings in size, each in a matrix with 5 total thicknesses from ~0.5 to ~1.5 Al extinction distances ( $\xi_{\text{Al}} = 24$  nm at 800 kV), and at three different depths for each size and each thickness. The largest supercells included ~70000 atoms. Each supercell was composed of a number of thin slabs with plane normal parallel to  $\langle 110 \rangle$ . Using CrystalKit, each slab was built to contain an AB stacking of Al atoms (2.86 Å thick), the smallest repeat distance along  $\langle 110 \rangle$  in Al. While the Al lattice repeats in each slab, the Pb lattice does not, due to the lattice mismatch between the two lattices and this was considered in creating subsequent slabs. Finally, the supercell was built by stacking all the slabs together thus creating 4 edge-on and 4 inclined interfaces. Atomic relaxation at the interfaces was not considered in these models. In order to test the visibility of steps at the interfaces, supercells containing an atomic ledge in one of the  $\{111\}$  interfaces were also built. Using NCEMSS running on a DEC Alpha station, image simulations were carried out for 9 defoci ranging from -30 nm to -110 nm.

36967                      A                      No

S. Paciornik, D. Michel and U. Dahmen

### **Refinement of Rigid Shift Component Normal to a $\Sigma 5$ Grain Boundary in Rutile by Quantitative HREM**

Proc. MSA 53 (submitted)

In the present work we describe a method for measurement of rigid shifts, that optimizes the fit between simulated and experimental images with respect to the magnitude of the rigid shift as a variable. The technique compares experimentally observed with modeled images using the normalized cross correlation coefficient as a measure for the goodness of fit. To avoid complications from elastic distortions, misorientations or extended relaxations, this optimization is applied only to a small segment of the image depicting a structural unit characteristic for the interface.

---

36968                      A                      No

R. Kilaas and S. Paciornik

### **The NCEM Public Domain Software Library of Extensions to Digital Micrograph**

Proc. MSA 53 (submitted)

A number of image processing algorithms have been developed at the NCEM as part of the ongoing research at the center. These routines are being made public in an effort to serve the electron microscopy community and will be made available through the NCEM world wide web home page. The first routines to be released all run under the Digital Micrograph image processing software from Gatan, Inc. and include extensions for peak-finding, lattice fit, displacement analysis, template matching, unit averaging and reduction of noise due to amorphous surface contamination.

B. Parvin, D. Agarwal, D. Owen, M.A. O'Keefe, K.H. Westmacott, U. Dahmen and R. Gronsky

### **A Project for On-Line Remote Control of a High-Voltage TEM**

Proc. MSA 53 (submitted)

A project has recently been established to provide users of the NCEM with remote on-line access to a 1.5MeV Kratos EM-1500 high-voltage transmission electron microscope via existing wide area networks. Within this project we are developing and implementing a set of tools, protocols, and interfaces to bring transmission electron microscopy on-line for collaborative research. Initially applied to the Kratos, the project will provide increased utilization of this unique instrument with its heretofore restricted access due to its sensitive components and demand for sophisticated operator skills. Additionally, the project will provide computer tools for capturing and manipulating real-time audio and video signals. These tools will be integrated into a standardized user interface that may be used for remote access to any transmission electron microscope equipped with a suitable control computer. This work is a first step towards a new kind of availability for unique microscopes located at central facilities. It will allow collaborations where multiple people at remote locations can monitor the experiments and discuss results while it is in progress. It will provide much greater accessibility to the microscope, and the new methods of controlling the microscope will greatly ease the operators task, leaving them free to concentrate on the science rather than the mechanics of running the microscope.

---

36989

A

No

Z. Weng-Sieh, R. Gronsky and A.T. Bell

### **Microstructural Evolution of $\gamma$ -Alumina Supported Rhodium Catalysts**

Proc. MSA 53 (submitted)

In an era of increasing environmental awareness, stricter federal and state regulation of pollutant emissions are emerging. A major source of pollution arises from automobiles which inadvertently form gaseous products such as nitric oxide, carbon monoxide, and hydrocarbons. Since the early 1980's these effluents have been converted to safer forms using a three-way catalytic converter that employs a high dispersion of rhodium and platinum particles supported on a large surface area of transitional  $\gamma$ -phase alumina. Unfortunately, such a converter is susceptible to decreased performance over time, and this degradation has been attributed to changes in the catalyst microstructure. The nanoscaled nature of the transition metal catalysts and the submicron-scaled size of the transitional alumina necessitates the use of the high spatial resolution analyses made possible by transmission electron microscopy.

---

M.A. O'Keefe

**Where are the Limits to Spatial Resolution in the HRTEM?**

Proc. MSA 53 (submitted)

The spatial resolution of a HRTEM is an upper bound on the resolution of images that can be produced by that microscope, with no guarantee that any particular image from the microscope will attain this bound. In addition to instrumental limits, specimen properties will degrade image resolutions. For specimens that beam-damage rapidly, image resolution depends upon electron energy and electron dose. For small-cell crystalline specimens, allowable resolutions will be quantized. "Resolution" has traditionally been defined in terms of the microscope's Scherzer resolution limit at optimum defocus. However, even beyond the Scherzer limit, it is possible to transfer spatial frequencies from the specimen to the image, out to the information limit of the electron microscope. The information limit measures the highest spatial frequency that can be transferred from the exit-surface wavefunction into an image, whereas the Scherzer resolution measures the highest spatial frequency that can be transferred into the image with the same phase as all lower frequencies contributing to that image. By successively tuning the HRTEM to pass different spatial frequency bands by choosing suitable defocus settings, then combining these images into one, we obtain a resolution that approaches the information limit of the microscope. With this technique a microscope's resolution will no longer be determined by its Scherzer limit, but will become identical to its information limit.

---

M.A. O'Keefe

**Advances in Image Simulation for High Resolution TEM**

Proc. MSA 53 (submitted)

Advances in image simulation have occurred on several fronts since mainstream application of image simulation to routine structure determination by HRTEM was ushered in by the SHRLI programs. There has been a steady improvement in modeling algorithms, including aberrations such as three-fold astigmatism. The most important advance is quantitative matching of simulated with experimental images. The experimental image is digitized, compared with simulations, and a "goodness-of-fit" parameter computed. For periodic specimens, comparison can be carried out in real space, by comparing the intensities of the images pixel by pixel, or in reciprocal space by comparing the image intensity spectra. The process can be automated and the simulation fit improved to yield the best matching image from a given model crystal structure. An automated two-step process can be used for refinement of an unknown structure, in the case where an experimental image is available with an unknown structure close to a known one. King and Campbell used an automated non-linear least-squares image-matching process to establish image parameters and refine the structure of a grain boundary, allowing the program to vary atom positions to achieve the best possible match and thus produce a refined structure model. Möbus and Rühle used a Gauss-Seidel bivariate search method to refine the structure of a niobium-sapphire interface.

---

37036

A

No

Z. Liliental-Weber, C. Kisielowski and J. Washburn

### **Chemical Sensitivity of Convergent Beam Electron Diffraction on the Stoichiometry of GaN**

Proc. MSA 53 (submitted)

III-V nitride thin film growth has attracted considerable attention because it now seems feasible to engineer semiconductor band gaps between 2.1 and 6.2 eV. One of the challenges coming with this development is related to the fact that structural perfection seems not to correlate directly with optical properties such as the emission of blue-green or UV light in GaN. In order to better understand this material, high resolution transmission electron microscopy (HREM) and convergent beam electron diffraction (CBED) experiments were used to study structural defects in GaN thin films. Experiments were performed with a Topcon 002B and ARM operating at 200 and 800 KeV, respectively, and were guided by image simulations.

---

37233

A

No

M.A. Wall, T.W. Barber Jr. and U. Dahmen

### **Techniques for In Situ HVEM Mechanical Deformation of Nanostructured Materials**

Proc. MSA 53 (submitted)

We have developed two *in situ* HVEM experimental techniques which allow us to begin fundamental investigations into the mechanisms of deformation and fracture in nanostructured materials. First, a procedure for the observation of tensile deformation and failure of multilayer (ML) materials in cross-section is detailed. Second, the development of an *in situ* HVEM nanoindenter of surfaces and films on surfaces in cross-section is presented.

**Superconductivity and Observation of Ordered Structures in Deintercalated  $\text{Li}_x\text{NbO}_2$** 

Proc. MSA 53 (submitted)

We have observed the appearance of extra reflections in [001] diffraction patterns obtained from deintercalated  $\text{Li}_x\text{NbO}_2$  materials, primarily a tripling along  $\langle 110 \rangle$  and a doubling along  $\langle 100 \rangle$ , and find the corresponding periodicities in high-resolution images. The occurrence of extra reflections in these diffraction patterns can be explained either by the presence of charge density waves in  $\text{Li}_x\text{NbO}_2$ , or by ordering of Li-vacancies after deintercalation. However, charge density waves are not expected to be stable in solids at room temperature, and we did not observe the development of any additional periodicities in a sample cooled to 100K. We thus attribute our images and diffraction patterns to the ordering of vacancies created as Li is removed from the host structure. The ordering of Li, apparently with two preferred periodicities, may be related to a phase separation revealed by magnetic measurement.

**High Voltage and High Resolution Electron Microscopy Investigation of Materials**

Proc. New Generation of HVEM 6 1995

An overview of the National Center for Electron Microscopy in Berkeley, emphasizes both our current research in materials sciences and instrumentation plans for the immediate future.

Z. Liliental-Weber, J. Ager, D. Look, X.W. Lin, X. Liu, J. Nishio, W. Swider, K. Wang, J. Washburn, E. Weber and J. Whitaker

## Structural Properties of the GaAs Layers Grown by MBE at Low Temperatures

Semi-Insulating III-V Compounds 305 1994

This paper describes the relation between structural properties of GaAs layers grown by MBE at low temperatures (LT-GaAs layers) before and after annealing. Conclusions are made based on x-ray, transmission electron microscopy (TEM), and carrier lifetime studies in combination with near-infrared absorption (NIRA), magnetic circular dichroism (MCD), and Raman spectroscopy measurements. To maintain consistency, the same samples have been studied using a variety of techniques. In this way it was shown that the expansion of the lattice parameter of these layers can be fully explained by the presence of the AsGa antisite defects. It was shown as well that the shortest carrier lifetime (200 fsc) was observed for as-grown samples grown at the lowest studied temperatures (190°-210° C), and that this time increased to 20 ps for growth temperatures up to 300° C.

---

35580

M

P

S. Im

## Ion Beam Synthesis of SiGe Alloy Layers

Ph.D. Thesis 1994

The synthesis of 200 nm thick SiGe alloy layers by implantation of high dose Ge ions with an incident energy of 120 keV into <100> oriented Si wafers yielded various Ge peak concentrations. After SPE annealing in a nitrogen ambient at 800° C for one hour, two kinds of extended defects were observed in alloy layers implanted at room temperature: end-of-range (EOR) dislocation loops and strain-induced stacking faults. The density of EOR dislocation loops was much lower in those alloys produced by liquid nitrogen temperature (LNT) implantation than by room temperature (RT) implantation. Decreasing the implantation dose to obtain 5 at% peak Ge concentration prevents strain relaxation showing high densities of misfit-induced stacking faults. Sequential implantation of C following high dose ( $5 \times 10^{16}/\text{cm}^2$ ) Ge implantation brought about a remarkable decrease in density of misfit-induced defects (stacking faults). When the nominal peak concentration of implanted C was greater than 0.55 at% stacking fault generation in the epitaxial layer was considerably suppressed. This effect is attributed to strain compensation by C atoms in the SiGe lattice. A SiGe alloy layer with 0.9 at % C peak concentration under a 12 at% Ge peak exhibited the best microstructure.

Please send a reprint of the paper(s):

Number	Author(s)	Title

Name\_\_\_\_\_ Date\_\_\_\_\_

Affiliation\_\_\_\_\_

Address\_\_\_\_\_

\_\_\_\_\_

Please send a reprint of the paper(s):

Number	Author(s)	Title

Name\_\_\_\_\_ Date\_\_\_\_\_

Affiliation\_\_\_\_\_

Address\_\_\_\_\_

\_\_\_\_\_

---

---

---

---

National Center for Electron Microscopy  
U.C. Lawrence Berkeley Laboratory  
1 Cyclotron Rd. Building 72  
Berkeley CA 94720

---

---

---

---

National Center for Electron Microscopy  
U.C. Lawrence Berkeley Laboratory  
1 Cyclotron Rd. Building 72  
Berkeley CA 94720

**National Center for Electron Microscopy  
Lawrence Berkeley Laboratory  
University of California  
Berkeley, Ca 94720**